NANOFLUID HEAT TRANSFER ENHANCEMENT IN ENGINEERING APPLICATIONS

BY

SURYA KUMAR SARIPELLA

B.Tech., Indian Institute of Technology Bombay, 2006
M.Tech., Indian Institute of Technology Bombay, 2006

THESIS

Submitted in partial fulfillment of the requirements
for the degree of Master of Science in Nuclear Engineering
in the Graduate College of the
University of Illinois at Urbana-Champaign, 2007

Urbana, Illinois

Advisers:

Professor Rizwan Uddin
Professor David M. France

NANOFLUID HEAT TRANSFER ENHANCEMENT IN ENGINEERING APPLICATIONS

Surya Kumar Saripella, M.S.
Department of Nuclear, Plasma and Radiological Engineering
University of Illinois at Urbana-Champaign, 2007
Dr. Rizwan-uddin, Adviser
Dr. David M. France, Co-Adviser (University of Illinois at Chicago)

In this study, the effect of nanofluid heat transfer enhancement in water based systems was investigated from an engineering system perspective. One such system considered was a "Class 8" truck, diesel engine cooling circuit using two different nanofluids to replace the conventional engine coolant. Results include quantifications of increase in engine heat rejection, reduction in truck frontal area and reduction in pumping power for the coolant circuit by the use of nanofluids instead of the conventional coolant.

"Nanofluid" refers to a fluid in which nanometer sized particles are suspended in a fluid, usually a liquid. Water based nanofluids have been considered as potential coolants for nuclear applications. In pool boiling situation, a critical heat flux enhancement of up to 200% have been reported. Potential benefits include increased safety margins in existing reactors and very high power density in PWRs. Nanofluids can also be used in Emergency Core Cooling Systems (ECCS) incorporated in both PWRs and BWRs.

Experiments were conducted at an experimental facility that has been developed at the Argonne National Lab to test heat transfer and flow characteristics of nanofluids have been used in this study. The experimental test section represented a second engineering

system considered in this study, and it was modeled using FLUENT® with the numerical results benchmarked to experimental observations for water as the working fluid. Subsequently, a nanofluid was simulated in FLUENT® and the performance compared to the base fluid of water.

Based on investigations pertaining to the "Class 8" truck diesel engine cooling circuit, modeled using FLOWMASTER®, it is observed that the coolant pump power can be reduced by a factor of eight, the engine heat rejection can be increased by up to 5%, and the frontal area of the truck can be decreased by up to 5%. Also, the engine temperature drops by up to 20% from the base case simulation.

The results obtained using the k-ω model in FLUENT® for water as the working fluid have been benchmarked using the experimental data from the nanofluid test facility at ANL. A nanofluid was simulated using FLUENT® to analyze potential enhancement. The results obtained using simulations show that though there is a decrease in the Nusselt number (~ 10%) when the base fluid is replaced with the nanofluid, the overall heat transfer coefficient increases (~ 30%) along with the increase in the thermal conductivity (~ 40%) of the working nanofluid.

Nanofluids have shown potential for enhancement in heat transfer in laboratory scale experimental investigations. An attempt has been made to quantify such claims for large engineering applications using numerical modeling as well as experimental

investigations. Results show significant potential for enhancement of heat transfer in engineering systems including nuclear applications.

Acknowledgement

I wish to take this opportunity to express my sincere gratitude towards my advisors Professor Rizwan-uddin and Professor David M. France for their valuable support throughout this project. Without their insight, guidance, patience and encouragement; this work would not have taken its present shape. I would also like to thank Professor Magdi Ragheb for his very valuable comments and suggestions, and for serving as the reader for this thesis.

I would also like to extend my gratitude towards Dr. Wenhua Yu, Dr. Fon-Cheih (Jimmy) Chang and Dr. Jules L. Routbort for their valuable guidance and timely help in the form important technical discussions during my summer internship at Argonne National Lab. I would like to specifically thank Mr. Roger K. Smith for his valuable technical assistance during the experimental analysis conducted at ANL.

I would also like to thank my family for their support and encouragement; without their love and patience, none of this would have been possible. Also, I would like to extend thanks to Suneet Singh, Rajneesh Chaudhary and Hitesh Bindra for their academic help and assistance, which has proved invaluable during the course of this project work. I would also like to appreciate: Prashant K. Jain, Rahul Samala, and Arpit Tiwari, for their friendship and support during my stay at UIUC. Finally, I would like to acknowledge all the faculty and staff of NPRE for their immense support, guidance, and wisdom.

Surya Kumar Saripella

Table of Contents

List of Figures

List of Tables

List of Acronyms

ANL	Argonne National Laboratory
BWR	Boiling Water Reactor
CFD	Computational Fluid Dynamics
CHF	Critical Heat Flux
ECCS	Emergency Core Cooling Systems
LWR	Light Water Reactor
NIST	National Institute of Standards
NSSS	Nuclear Steam Supply System
NPP	Nuclear Power Plant
NTU	Number of Transfer Units
PWR	Pressurized Water Reactor
RPM	Revolutions Per Minute
TER	Thermal conductivity Enhancement Ratio

Chapter 1

Introduction

A large number of nuclear thermal-hydraulic processes involve the transfer of heat by incorporating flowing fluids, sometimes boiling, in both the laminar and turbulent flow regimes. To enhance heat transfer, a wide range of different fluids and operating conditions (including temperature and pressure) are tested and used. These applications would benefit from improved heat transfer properties like the reduced thermal resistance of the working fluid. Implementation of such fluids into the existing systems can lead to a reduction in the capital costs, improved working efficiency and also in better design of the overall system.

Nanofluids, with their reduced thermal resistance and improved heat transfer properties, are a potential choice for these working fluids. There are a large number of engineering systems like transportation, electronics, medical, manufacturing as well as nuclear engineering that can take advantage of such fluids. Although much of the nanofluid research is conducted outside the field of nuclear engineering, the results may often be applicable to nuclear reactor systems. Some specific systems are discussed in section 1.5.

"Nanofluid" refers to a fluid in which nanometer sized particles are suspended in a fluid, usually a liquid [Choi 1995; Lee 1999]. Nanofluids with such suspended particles have been shown to enhance the convective heat transfer performance as well as the thermal

conductivity compared to the respective base fluids (typically the existing working fluids). The fundamental idea behind the enhancement of thermal conductivity is owing to the fact that the thermal conductivity of the suspended particles (typically metal-oxides) is an order of magnitude higher than that of the base fluids like water, ethylene glycol, etc; hence, the enhancements in the heat transfer performance of the overall system.

Nanotechnology based *designer* fluids developed by stably suspending nanoparticles (typically of length 1-100 nm) in conventional heat transfer liquids are termed as nanofluids. Review papers [Choi et al. 2004; Eastman et al. 2004; Keblinski et al. 2005; Das et al. 2006; Das 2006] include various aspects of this new research field including the history of technology development. It is clear that these technologically enhanced fluids have thermal properties that may be quite different from their base fluid. It has been shown that in one of the cases a small amount (less than 1% by volume) of addition of nanoparticles to the fluid in one case increased the thermal conductivity by a factor of two [Choi et al. 2001]. As will be discussed later, experiments have shown that the thermal conductivity is enhanced, in general, from 15-40% with nanoparticle volume concentrations of 0.5 - 4% in the base fluid.

The characteristic features of the nanofluids include:

1) Significant increase in the thermal conductivity with low volume concentrations [Choi et al. 2001].

2) Stronger dependence of thermal conductivity on temperature than the base-fluid alone [Das et al. 2003].
3) Increased critical heat flux for pool boiling scenarios [You et al. 2003].
4) Substantial increase in heat transfer coefficient [Yu et al. 2007].

Thermal conductivity and heat transfer coefficient are the defining parameters for coolant fluids. From the literature available, it is apparent that the reported enhanced heat transfer rates are beyond just the effect of enhanced thermal conductivity [Das et al. 2006a]. Though different mechanisms have been proposed, the scientific community still does not agree on an explanation as to how the nanoparticles enhance the heat transfer properties of the fluid.

1.1 Overview of the thesis

In the following sections of the coming chapter, we take a glance at the literature review relevant to the field of thermal enhancement pertaining to nanofluids. Literature pertaining to experimental observations of thermal conductivity and heat transfer coefficient enhancement has been studied. Specific applications related to the general area of nuclear engineering have also been identified in this chapter.

In chapter 2, we look at the specific case of nanofluids as potential coolants for a specific case of "Class 8" truck coolant circuit. Various parametric studies have been performed using the commercial code viz. FLOWMASTER to improve the performance of the existing coolant system. Specific studies include:

1) Increasing engine heat rejection to coolant circuit.

2) Reducing the radiator air-side area.

3) Reduction in pump power and speed.

In chapter 3, a few experimental results corresponding to tests performed at the nanofluid heat transfer test facility at ANL have been presented. The experimental test-section is modeled in FLUENT®. Furthermore, comparisons are made using the k-omega turbulence model, between the base fluid and corresponding nanofluid for various flow cases using FLUENT®. Results related to potential heat transfer enhancement as predicted using the turbulence model have been presented.

Finally, a few conclusions with regard to the potential of nanofluids and scope for future work in this exciting area of research have been discussed in chapter 4.

1.2 Experimental research on nanofluid thermal conductivity

To understand the heat transfer enhancement in a nanofluid, a first step is to analyze the behavior of the thermal conductivity of such fluids. The physical mechanism for heat transfer enhancement in nanofluids is not very well understood. One of the first analytical models for heat transfer of fluids with suspended particles was given by Maxwell [Maxwell 1873]. In this model, the fluid is considered to have suspended spherical particles with no interaction among themselves. The Maxwell equation for thermal conductivity is given by:

$$k_e = k_m + 3v_p \frac{k_p - k_m}{2k_m + k_p - v_p(k_p - k_m)} k_m \qquad (1.1)$$

In the above equation k_e is the effective conductivity of the nanofluid; k_m is the conductivity of the base fluid; v_p is the particle concentration fraction and k_p is the thermal conductivity of the nanoparticles. The Maxwell's model assumes that the particles are small spheres and that the concentration is low. From Maxwell's model, for enhanced thermal conductivity, $k_p > k_m$ which suggests that the thermal conductivity of nanoparticles must be larger than the conductivity of the base fluid. This may preclude its applicability to nuclear reactors with liquid metal coolants like Sodium.

A large number of extensions and modifications to the Maxwell's equation have been suggested based on various experimental facts observed. The suggested extensions/modifications take the following effects into account:

- Particle shape [Fricke 1924; Fricke 1935; Polder and van Santen 1946; Hamilton and Crosser 1962; Taylor 1965; Taylor 1966; Granqvist and Hunderi 1977; Granqvist and Hunderi 1978; Xue 2000].
- Particle size distribution [Rayleigh 1892; Wiener 1912].
- High volumetric concentration [Bruggerman 1935; Böttcher 1945; Landauer 1952; Jeffrey 1973; Davis 1986].
- Particle Shell structure [Xue 2000; Kerner 1956; Van de Hulst 1957; Pauly and Schwan 1959; Schwan et al. 1962; Lamb et al. 1978; Benveniste and Miloh 1991; Lu and Song 1996].
- Contact Resistance [Benveniste 1987; Hasselman and Johnson 1987].

The predictions made by the models give satisfactory results for dilute mixtures with relatively large particles in solution, but the comparison has not been very satisfactory between experimental data and theoretical predictions for nano-scale particle suspensions. Specific mechanisms have been identified and formulated in the models for the nanoscale phenomena to improve predictions. These include the effects of nanoparticle-matrix interfacial layer [Yu and Choi 2003; Yu and Choi 2004; Xie et al. 2005; Ren et al. 2005], nanoparticle Brownian motion [Xuan and Li 2003; Jang and Choi 2004; Koo and Kleinstreuer 2004; Prasher et al. 2005; Prasher et al. 2006a], and nanoparticle cluster/aggregate [Wang et al. 2003; Prasher et al. 2006b]. Results from these models agree with limited data, and to date, no universally agreed theory to predict the thermal conductivity of nanofluids exists.

The Thermal conductivity Enhancement Ratio (TER), or simply enhancement, is defined as the ratio of the nanofluid effective thermal conductivity to the thermal conductivity of the base fluid. From Eq. (1.1) we can show that:

$$\mathrm{TER} = \frac{k_e}{k_m} = 1 + 3v_p \frac{k_p - k_m}{2k_m + k_p - v_p(k_p - k_m)} \qquad (1.2)$$

Experimental studies have shown the effects of eight parameters which enhance the nanofluid conductivity viz. [Yu et al. 2007].

1) Particle volume concentration.
2) Particle material properties.
3) Particle size.
4) Particle shape.
5) Base fluid material properties.

6) Temperature.

7) Additives (like surfactants etc.).

8) Acidity (pH of the nanofluid).

1.3 Experimental research on heat transfer

An increase in thermal conductivity coupled with changes in viscosity, density and specific heat are indications for an improved heat transfer behavior of the fluid. For heat transfer applications, a more important parameter would be the heat transfer coefficient of the nanofluid. Improvement in the heat transfer coefficient would lead to a reduction in the size of systems and increased energy and fuel efficiencies. To this end, it is most important to measure the heat transfer coefficients of nanofluids under similar flow conditions as base fluids to understand the impact and hence the respective enhancement.

Nanofluid heat transfer enhancement is typically divided into three broad areas viz., laminar flow, turbulent flow and pool boiling. In this study, single-phase flow was considered, and heat transfer enhancement was paramount. An important detailed body of experimental work pertaining to alumina (Al_2O_3) nanoparticles suspended in water has been performed by various researchers [Xie et. al. 2002a; Xie et al. 2002b; Xie et al. 2002c; Yang and Han 2006]. The heat transfer enhancement increases as does the thermal conductivity of the nanofluids compared to their base fluids. Some of these experimental results suggest that the heat transfer enhancement is higher than the thermal conductivity enhancement and hence this area has developed a keen interest among researchers. These

findings tend to suggest that presence of nanoparticles in the flow influences the heat transfer beyond the expected thermal conductivity enhancement.

1.4 Nanofluids with suspended metal-oxide nanoparticles as fluids for enhanced heat transfer applications

Based on the experimental research discussed above, nanofluids have shown the potential for enhancement both in thermal conductivity and in overall heat transfer aspects for various flows. This has suggested that the convective heat transfer process can be improved using nanofluids in a variety of engineering systems. Typically metal-oxide nanoparticles (like CuO, Al_2O_3, TiO_2, etc.) are used to prepare such nanofluids with enhanced heat transfer properties. Researchers [Pak and Cho 1998] have quantified the heat transfer enhancement of such water based nanofluids with metal oxide nanoparticles. Results have been published in the engineering literature related for CuO in water [Lee et al. 1999; Wang and Choi 1999], CuO in ethylene glycol [Lee et al. 1999; Wang and Choi 1999], and Al_2O_3 in water [Lee et al. 1999; Das et al. 2003] for enhancements in the heat transfer properties. The nanofluids with CuO particles in water and ethylene glycol are of direct interest to the automotive industry because a mixture of ethylene-glycol and water is used as a coolant for various engines. Heat transfer enhancement in laminar flows for CuO particles in water has been measured to be in the ranges from 1.02 – 1.38 [Herris et al. 2006]. Turbulent flow heat transfer enhancements for Al_2O_3 and TiO_2 in water have been reported as 1.07 - 1.35 and 0.93 - 1.20 [Pak and Cho 1998]. Based on

these findings, there is potential for metal-oxide based nanofluids for heat transfer enhancement applications.

1.5 Nanofluids as potential coolants for nuclear reactors

Water based nanofluids have been considered as potential coolants for nuclear applications [Boungiorno and Hu 2005]. The presence of nanoparticles enhances energy transport resulting in higher thermal conductivity and heat transfer coefficients than water alone. In a pool boiling situation with small concentrations of alumina and silica nanoparticles (< 0.001% vol.), a critical heat flux (CHF) enhancement of up to 200% in water based nanofluids has been reported [Yu et al. 2003; Yu et al. 2004]. These results have raised the curiosity among the nuclear engineering community to harness the potential of nanofluids and use them to improve reactor heat transfer efficiency.

Potential benefits of nanofluids include increased safety margins in existing PWRs and very high power density in innovative PWRs [Boungiorno and Hu 2005]. The advantages for using these fluids lie in more than one aspect viz. increased thermal conductivity, improved single phase heat transfer and increase in the critical heat flux. Analytical studies have shown that using a nanofluid coolant in a PWR can increase the heat flux density by up to 40%. Also, a CHF increase of 30% is an added advantage [Boungiorno 2005].

Nanofluids can also be used in the Emergency Core Cooling Systems (ECCS) incorporated in both PWRs and BWRs. Nanofluids have the potential to increase the heat

transfer rates by up to 40% and hence hasten the process of cooling, thus improving safety for the emergency cooling system. Nanofluids are also being considered as potential coolants for in-vessel retention of a molten core during a hypothetical severe accident scenario in high power density LWRs [Boungiorno et al. 2006].

While there are potential benefits of nanofluids, there are also sources for concern. These must be adequately assessed before nanofluids are introduced in any engineering system. For example, one of the potential concerns with metal-oxide nanoparticles (like CuO, Al_2O_3, TiO_2 etc.) would be their exposure to high neutron fluxes in nuclear reactor cores and subsequent neutron activation of these metals. In some cases radioactive decay and formation of potentially hazardous isotopes is possible. For example neutron activated Copper undergoes beta decay and also releases gamma radiation on its way to becoming Vanadium. However, the elements such as Aluminum and Titanium tend to form stable isotopes even after undergoing neutron activation.

Another potential negative impact of nanofluid is the possibility of clogging and erosion within the system due to their use. Problems related to coagulation of nanoparticles have been observed with nanofluids. Such coagulation often results in formation of precipitates which may lead to clogging of the cooling system and hence poses potential danger to the overall system. Further experimental investigations regarding the stability of nanofluids as well as their potential to erode the piping need to be carried out before any such fluids are incorporated into practical systems.

Chapter 2

Nanofluids as coolant for improved heat transfer

The objective of this effort was to study the effect of nanofluids as potential coolants in engineering systems including nuclear related applications. As an example of a relatively complex heat generating system that needs to be cooled, simulations have been carried for a truck engine coolant system. Just as in Nuclear Steam Supply System (NSSS) and other parts of a Nuclear Power Plant (NPP), the efficient design of a coolant circuit is an important component of the engine design procedure. The coolant determines the maximum temperature in the engine and helps remove the excess heat generated due to combustion and dissipate it. Utilizing the one-dimensional system capabilities of FLOWMASTER®, a system simulation software tool designed to simulate and analyze complex thermal and fluid systems, various components can be sized for tighter packaging and improved performance keeping the optimum permissible temperature levels for the engine. (Additional details about FLOWMASTER® are given in Section 2.4.) The simulation was carried out to quantify improvements in performance when a nanofluid is used over an ordinary fluid. The primary goals of the numerical modeling effort are:

- Compare the performance of nanofluids as potential coolants compared to conventional coolants for a “Class 8” Truck diesel engine.
- Study the performance and sizing of the pump and radiator to maximize the cooling effect and minimize power consumption under steady-state conditions.

- Estimate the enhancement in cooling capacity of the coolant circuit for a given design.

Note that very similar simulations, using a nuclear systems code, can be carried out to analyze the corresponding conditions in a nuclear power plant.

2.1 Nanofluid coolants

In the automotive industry, large over-the-road truck cooling systems use an ethylene-glycol/water (50/50) by volume (%) mixture as the coolant fluid in their coolant circuits. In the current study, two nanofluids were considered.

1) 2% by volume of CuO nanoparticles + ethylene-glycol/water (50/50)
2) 4% by volume of CuO nanoparticles + ethylene-glycol/water (50/50)

Sometimes, for stability of the nanofluids, some surfactants may be added to this system.

2.2 Calculation of physical properties of nanofluids

The various properties of the nanofluid can be calculated from the base fluid and the particles using the following equations for the effective density (ρ_e), viscosity (μ_e) and the specific heat (C_{pe}) :

$$\rho_e = (1-v_p)\rho_m + v_p\rho_p \qquad (2.1)$$

$$C_{pe} = \frac{(1-v_p)(\rho C_p)_m + v_p(\rho C_p)_p}{(1-v_p)\rho_m + v_p\rho_p} \qquad (2.2)$$

$$\mu_e = (1+2.5v_p)\mu_m \qquad (2.3)$$

where '*m'* represents the base fluid, '*p'* represents the particle and '*e'* represents the effective nanofluid property. The effective density, specific heat and viscosity are calculated as shown from equations 2.1-2.3. The viscosity is dependent on the particle density (by volume percentage) [Einstein 1906] as shown in equation 2.3, above.

Table 1. Density and specific heat of nanofluid with 2% and 4% of CuO nanoparticles as a function of temperature

Fluid		Ehtylene-Glycol/Water (50/50)		Nanofluid with 4% CuO nanoparticles by volume		Nanofluid with 2% CuO nanoparticles by volume	
	Temperature (^{0}C)	Density (kg/m^3)	Specific Heat (kJ/kg-K)	Density (kg/m^3)	Specific Heat (kJ/kg-K)	Density (kg/m^3)	Specific Heat (kJ/kg-K)
1	-20	1091	3.005	1303.36	2.5144	1197.18	2.7379
2	-10	1087	3.087	1299.52	2.5799	1193.26	2.8108
3	0	1082	3.165	1294.72	2.6417	1188.36	2.8799
4	10	1078	3.236	1290.88	2.6981	1184.44	2.9429
5	20	1072	3.303	1285.12	2.7504	1178.56	3.0017
6	30	1067	3.365	1280.32	2.7990	1173.66	3.0563
7	40	1061	3.421	1274.56	2.8423	1167.78	3.1052
8	50	1055	3.472	1268.8	2.8815	1161.9	3.1496
9	60	1048	3.517	1262.08	2.9154	1155.04	3.1883
10	70	1042	3.558	1256.32	2.9463	1149.16	3.2236
11	80	1035	3.593	1249.6	2.9720	1142.3	3.2533
12	90	1027	3.623	1241.92	2.9931	1134.46	3.2782
13	100	1020	3.648	1235.2	3.0106	1127.6	3.2989
14	110	1012	3.667	1227.52	3.0228	1119.76	3.3139
15	120	1003	3.682	1218.88	3.0312	1110.94	3.3250

Using the above relations, the properties of the nanofluid can be calculated as a function of temperature. The thermal conductivity and heat transfer coefficient cannot be written down as direct expressions but are typically found experimentally. It has been observed that the thermal conductivity for 2 volume % of CuO nanoparticles increases by about 20% and for the 4 volume % concentration of CuO it is enhanced by about 40% with respect to the base fluid.

Table 2. Thermal conductivity of nanofluid with 2% and 4% of CuO nanoparticles as a function of temperature

		Thermal Conductivity (W/m-K)		
Serial No.	Temperature (^{0}C)	Ethylene-Glycol/Water (50/50)	Nanofluid with 4% CuO nanoparticles by volume	Nanofluid with 2% CuO nanoparticles by volume
1	-20	0.276903	0.3876642	0.3322836
2	-15	0.278714	0.3901996	0.3344568
3	-10	0.280516	0.3927224	0.3366192
4	-5	0.282279	0.3951906	0.3387348
5	0	0.283998	0.3975972	0.3407976
6	5	0.285666	0.3999324	0.3427992
7	10	0.287274	0.4021836	0.3447288
8	15	0.288822	0.4043508	0.3465864
9	20	0.290308	0.4064312	0.3483696
10	25	0.291731	0.4084234	0.3500772
11	30	0.293092	0.4103288	0.3517104
12	35	0.294389	0.4121446	0.3532668
13	40	0.295621	0.4138694	0.3547452
14	45	0.296788	0.4155032	0.3561456
15	50	0.297888	0.4170432	0.3574656
16	55	0.29892	0.418488	0.358704
17	60	0.299884	0.4198376	0.3598608
18	65	0.300779	0.4210906	0.3609348
19	70	0.301603	0.4222442	0.3619236
20	75	0.302355	0.423297	0.362826
21	80	0.303035	0.424249	0.363642
22	85	0.303642	0.4250988	0.3643704
23	90	0.304173	0.4258422	0.3650076
24	95	0.304628	0.4264792	0.3655536
25	100	0.305007	0.4270098	0.3660084
26	105	0.305306	0.4274284	0.3663672
27	110	0.305526	0.4277364	0.3666312
28	115	0.305665	0.427931	0.366798
29	120	0.305722	0.4280108	0.3668664
30	125	0.305695	0.427973	0.366834
31	130	0.305583	0.4278162	0.3666996
32	135	0.305384	0.4275376	0.3664608
33	140	0.305097	0.4271358	0.3661164

The corresponding numerical values are given in Tables 1, 2 and 3. Table 1 shows the specific heat and density changes for the nanofluids with respect to the corresponding base fluid as functions of temperature. Properties of the base fluid are taken directly from the data being given as input to the FLOWMASTER® code [Flowmaster Inc.].
Table 2 shows the thermal conductivity, as a function of temperature for the base fluid and for the two nanofluids modeled for the truck.

The dynamic viscosity as a function of temperature (Table 3) is calculated for the nanofluids using the Einstein approximation [Einstein 1906], Eq. (2.3).

Table 3. Viscosity of nanofluid with 2% and 4% of CuO nanoparticles as a function of temperature

		Dynamic Viscosity (kg/m-s)		
Serial No.	**Temperature (^{0}C)**	**Ethylene-Glycol/Water (50/50)**	**Nanofluid with 4% by volume of CuO nanoparticles**	**Nanofluid with 2% by volume of CuO nanoparticles**
1	-20	0.02645	0.029095	0.0277725
2	-10	0.01632	0.017952	0.017136
3	0	0.01032	0.011352	0.010836
4	10	0.006748	0.0074228	0.0070854
5	20	0.004588	0.0050468	0.0048174
6	30	0.003243	0.0035673	0.00340515
7	40	0.002376	0.0026136	0.0024948
8	50	0.001814	0.0019954	0.0019047
9	60	0.001425	0.0015675	0.00149625
10	70	0.001177	0.0012947	0.00123585
11	80	0.001004	0.0011044	0.0010542
12	90	0.000883	0.0009713	0.00092715
13	100	0.000816	0.0008976	0.0008568
14	110	0.000779	0.0008569	0.00081795
15	120	0.000772	0.0008492	0.0008106

2.3 Coolant system modeling

A general purpose simulation tool called FLOWMASTER® has been used in this study to analyze the coolant system. FLOWMASTER® is a system simulation software tool designed to simulate and analyze complex thermal and fluid systems. This one-dimensional system modeling package includes wide ranges of system specific components enabling the user to build networks and understand steady state and transient behavior of the overall system. The post-processing features in the code include the ability to understand the numerical results for each specific component, hence enhancing the capability to interpret the results. (Flowmaster Inc.)

Attempt to solve the flow and temperature distributions through the coolant circuit using a direct steady state solver led to convergence problems. The problems arose owing to the non-linearity due to the temperature dependent properties of the working coolant and also due to the components like the thermostat which redistribute the flow between two paths based on the temperature of the fluid at the inlet of the component. Hence, a *pseudo-transient* analysis was used to analyze the performance of the coolant circuit under steady state conditions. In a pseudo-transient analysis, we look at the transient behavior of the system starting with a realizable initial condition. The results of the simulation after a sufficiently large simulation time would match the steady state results for the given system.

An initial condition was chosen, starting at the ambient temperature conditions for all components in the system as this is a physically realizable scenario where the truck is at

rest. Starting from such an initial condition, the system is analyzed at a point of time when there is almost no change in the solution with time. This represents the steady state solution for the given system.

2.4 System description

A one dimensional model for simulating a common automotive coolant system is developed with the help of FLOWMASTER®. The current model incorporates the various systems used in the current designs of truck engines. The current model, developed in FLOWMASTER®, includes the heat rejection from the engine to the coolant circuit and from the coolant to air in the radiator. The coolant pump drives the flow through the network and the thermostat distributes the coolant between the radiator and the bypass circuits based on the actuation temperature. The circuit can be divided into six major subsystems:

1) Engine
2) Thermostat
3) Pump
4) Radiator and expansion tank
5) Radiator bypass
6) Cabin heater

A complete cooling system block diagram is shown in Figure 1

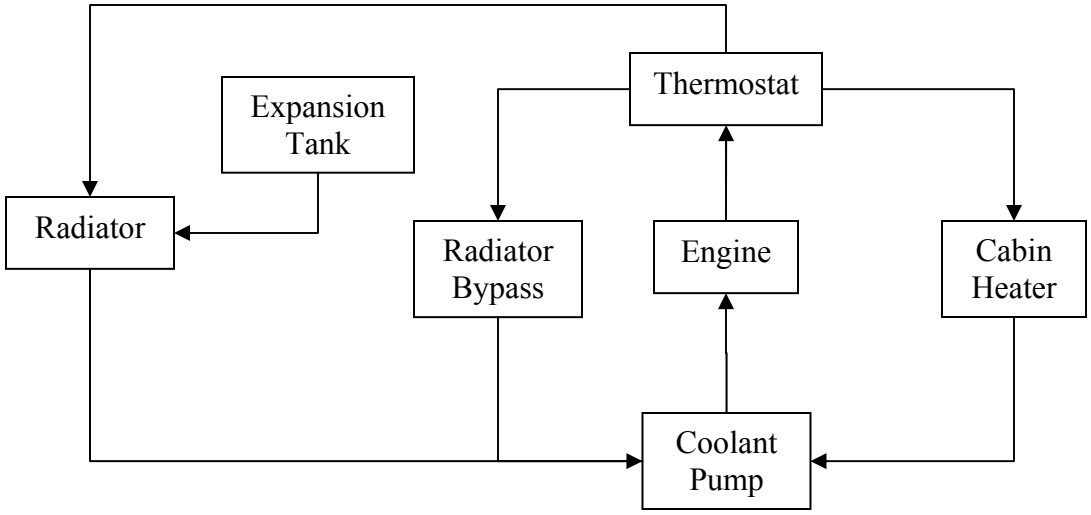

Figure 1. Block diagram for a truck coolant system

The cabin heater under the summer time conditions is typically turned off. In the winter case, there is a valve which directs coolant flow through the cabin heater section of the coolant circuit.

The system, as modeled in FLOWMASTER® is shown in Figure 2. The system components are discussed individually in the next sections.

2.4.1 Engine system

The engine acts as a source of heat to the coolant circuit which the coolant rejects in the radiator. This source is modeled as a combination of a point mass and a heat flow source.

a) *Heat flow source* – This represents the heat rejected to the coolant circuit due to combustion. This could, in general, be a time-dependent quantity.

b) *Point mass* – The point mass is used to represent the overall mass of the engine block. The material properties of the overall engine are taken into consideration here and this helps in transient analysis to estimate the temperature of the engine.

c) *Thermal bridge* - The thermal bridge acts as the point of connection between the coolant circuit and the engine. The heat flows from the engine into the coolant circuit at the thermal bridge. This is used to model the various flow-paths within the engine of the coolant. The thermal bridge is a computational modeling technique used by FLOWMASTER® rather than an actual physical system component.

2.4.2 Thermostat

The thermostat has been modeled using two globe valves in conjunction with an operational variable controller. The thermostat valve controller is used to control the degree of opening of the two ball valves based on the temperature of the coolant flowing into the thermostat in the circuit. Over an input temperature range, the thermostat increases the flow of the coolant to the radiator and decreases the by-pass flow.

2.4.3 Pump system

The coolant pump for the system is represented as a mixed flow pump along with a pump speed controller.

a) *Mixed flow pump* – This requires the input of the rated operating conditions for the pump such as power, flow rate, speed and head. Based on a normalized performance curve for the pump, the various conditions at the point of operation are calculated internally.
b) *Pump speed controller* – The speed controller changes the speed of the pump as a function of time for transient characteristics.

2.4.4 Radiator and expansion tank

The radiator in an automotive engine is essentially a cross-flow heat exchanger. The expansion tank acts as a reservoir for the coolant within the circuit.

a) *Radiator*- An automotive radiator is a cross-flow heat exchanger between the coolant and the ambient air. This component couples the fluid flow effects viz. pressure drop along with the heat transfer characteristics.
b) *Fan*- The fan is used to charge the ram air (which is the incoming air which is charged up due to the relative motion between the truck and the surroundings) to increase the air velocity before entering the radiator. This helps in improving the radiator performance.
c) *Air side circuit*- The air side of the radiator is modeled using a pressure inlet coupled with a flow source. The flow rate is specified based on the radiator air side area and the flow velocity of the incoming air.

d) *Expansion tank*-The expansion tank acts as a reservoir for the coolant in the coolant circuit. When the engine is not in operation, the coolant is at ambient temperature conditions. During operation, the coolant reaches much higher temperatures of the order of 80-110 ^{0}C. The extra volume of the coolant, due to thermal expansion, goes to the expansion tank and again comes back to the coolant loop once the engine stops running and the coolant cools back to room temperature.

2.4.5 Radiator bypass system

In a truck, the thermostat allows the coolant to pass through the radiator only after it reaches a certain temperature. Before this temperature is attained, the coolant flow bypasses the radiator system. This is modeled using an orifice in a bypass circuit. The orifice is designed so as to have a similar pressure drop as the radiator loop. This helps in achieving a stable numerical solution without numerical instabilities (oscillations).

2.4.6 Cabin heater circuit

In winter conditions, the heating within the cabin is achieved by transferring heat from the coolant of the engine to the cabin in the vehicle. The cabin heater consists of a ball valve and a heat exchanger.

a) *Ball valve*- The ball valve is used to turn on/off the cabin heater circuit. During summer conditions, it is turned off, otherwise it is kept open. Typically, in a vehicle this is a manual control provided to the user.

b) *Heat exchanger*- This represents the cabin heater section which allows for heat transfer between the cabin air and the coolant. This also accounts for the pressure drops based on the flow rates on both sides.

c) *Three-way junction*- The three way junction helps to determine the percentage of outside air going to the cabin heater out of the total air flow. This is generally a manual control available within the vehicle.

d) *Air side circuit*- As with the radiator, the air side of the heat exchanger is modeled using a pressure inlet and a flow source.

All of the components described above make up the FLOWMASTER® model of the "Class 8" diesel truck engine cooling system. The model is shown schematically in Fig. 2 in the form that it is input to FLOWMASTER®.

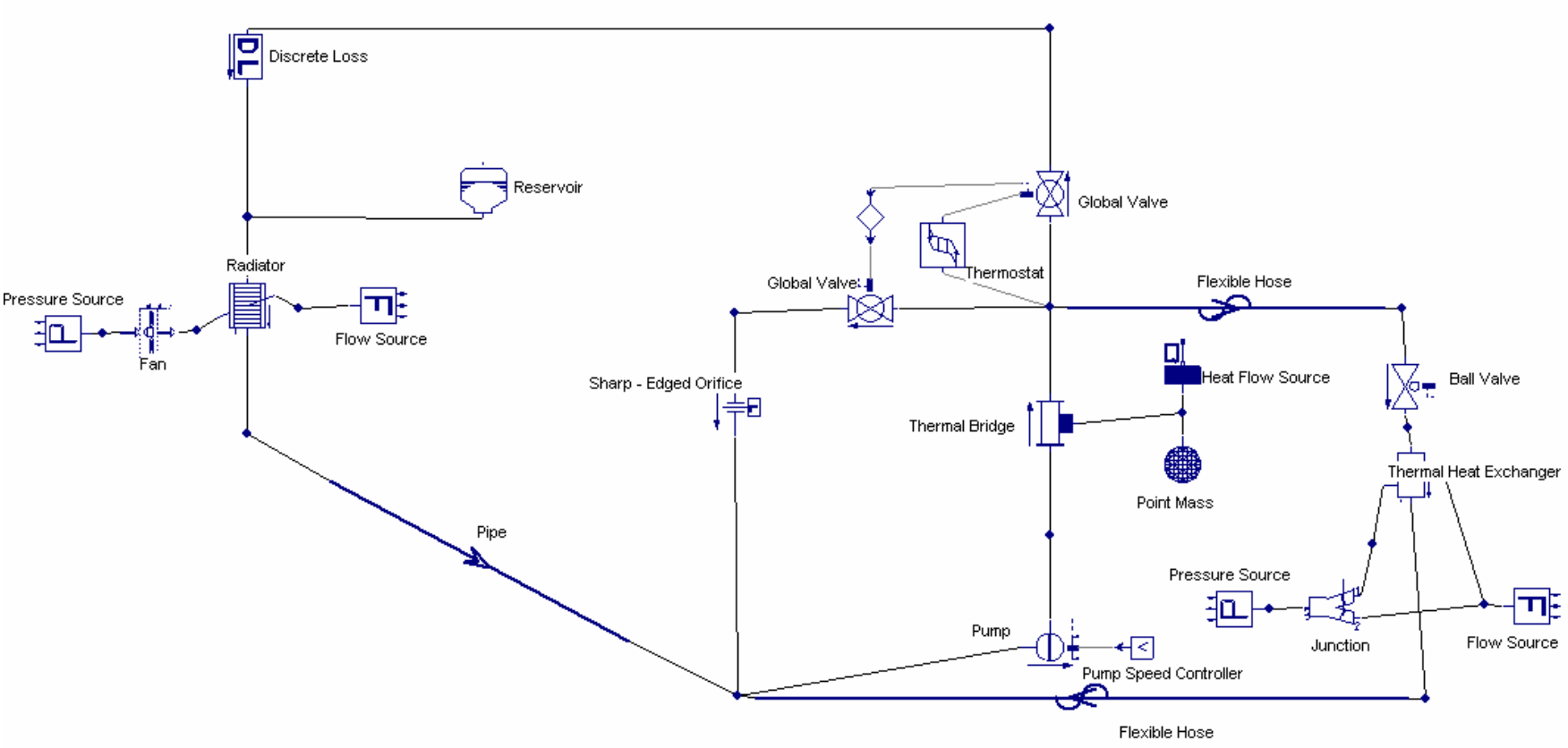

Figure 2. Coolant circuit diagram as modeled in FLOWMASTER

2.5 Coolant circuit component parameter details

In this section, the details of all component inputs to FLOWMASTER are given. Most of the information was determined from a generic "Class 8" Truck diesel engine. Parameters were chosen comprising the coolant system design point where the maximum heat rejection is required under the most restrictive condition. For a large truck, that design point corresponds to climbing a steep grade in the summer in a desert climate.

1. *Engine heat rejection*: The heat rejection for a truck diesel engine to the coolant circuit was set to 298.4 kW (400 hp) at its peak point. This relates to a practical scenario where the truck is going up a steep grade and the engine is working at its maximum power conditions. It corresponds to an engine rated at about 372.85 kW (500 hp). For the pseudo-transient analysis, the engine heat rejection is increased to its maximum value of 400 hp over time as shown in Fig. 3.

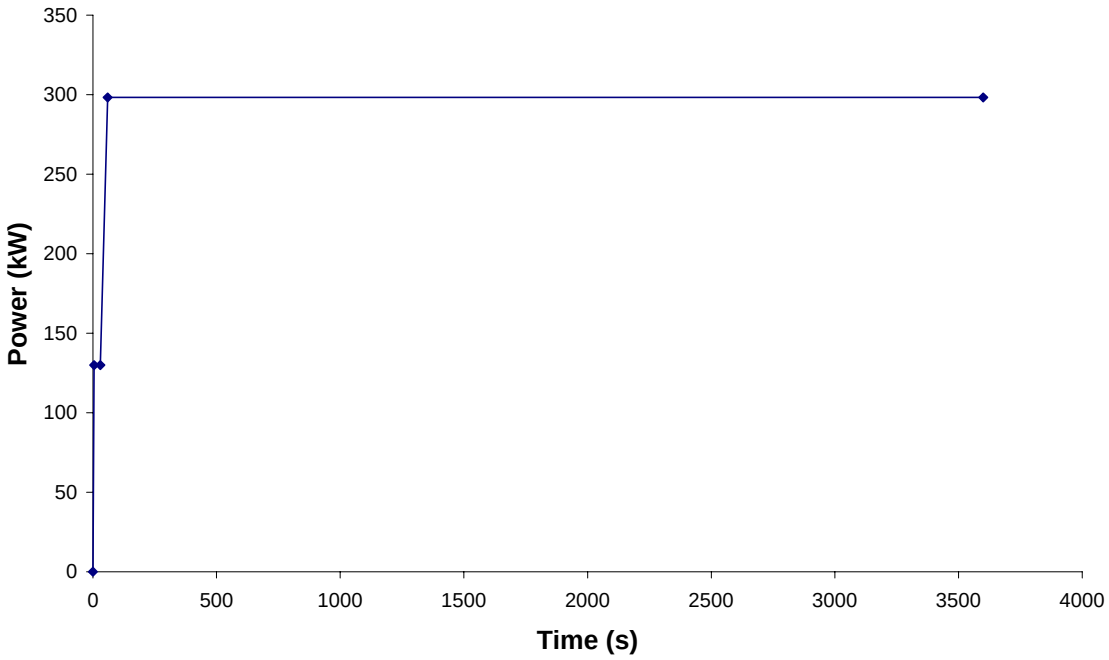

Figure 3. Engine heat rejection as a function of time

2. *Thermostat*: The thermostat in a truck diesel is set to open at a temperature of about 82 ^{0}C. It is completely open by about 92 ^{0}C. The thermostat valve opening can be given as a plot input to FLOWMASTER® as shown in Fig. 4.

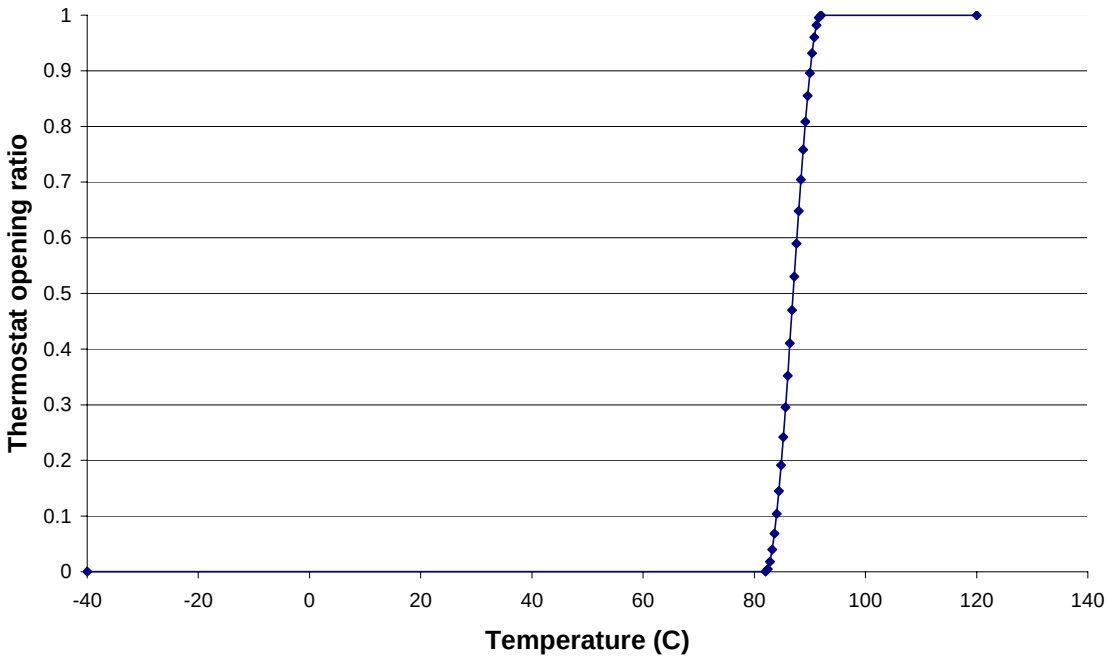

Figure 4. Thermostat opening as a function of temperature

3. *Pump speed control*: The pump is controlled by a speed controller. In practice, the pump is coupled with the engine speed and there is no separate control. In the code, as the engine speed is not modeled, a separate pump speed controller is provided. This is used only for the pseudo-transient purposes and is only a feature of the model. For the base case scenario, the pump runs at 1600 RPM at the steady state and the corresponding pump speed control plot has been shown in Fig. 5.

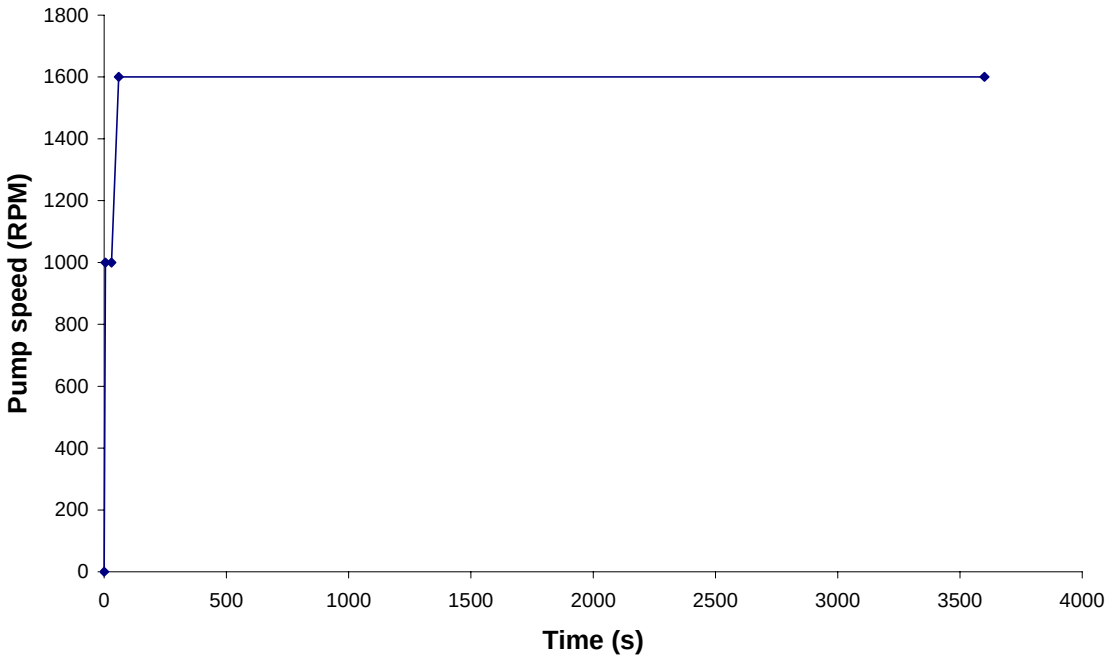

Figure 5. Pump speed as a function of time

4. *Radiator and cabin heater effectiveness*: The radiator is a cross-flow heat exchanger. The effectiveness of a heat exchanger can be expressed as a function of the mass flow rates of both the sides. The commercial code FLOWMASTER has the capability of taking in the effectiveness as a function of mass flow rates on both sides (or the respective volumetric flow rates) and then interpolating to find intermediate values for the same. The effectiveness curves for both the radiator and the cabin heater are incorporated into the circuit (see Figs. 6 and 7 for the radiator and cabin heater, respectively). The cabin heater effectiveness is taken from the generic data available for a cabin heater within FLOWMASTER®. The effectiveness values for the radiator are calculated and are presented in Table 4. For the summer ambient conditions, the cabin heater is essentially shut-off. Only

the results for the summer scenario were addressed in this study because the peak load design conditions are attained at that time of the year.

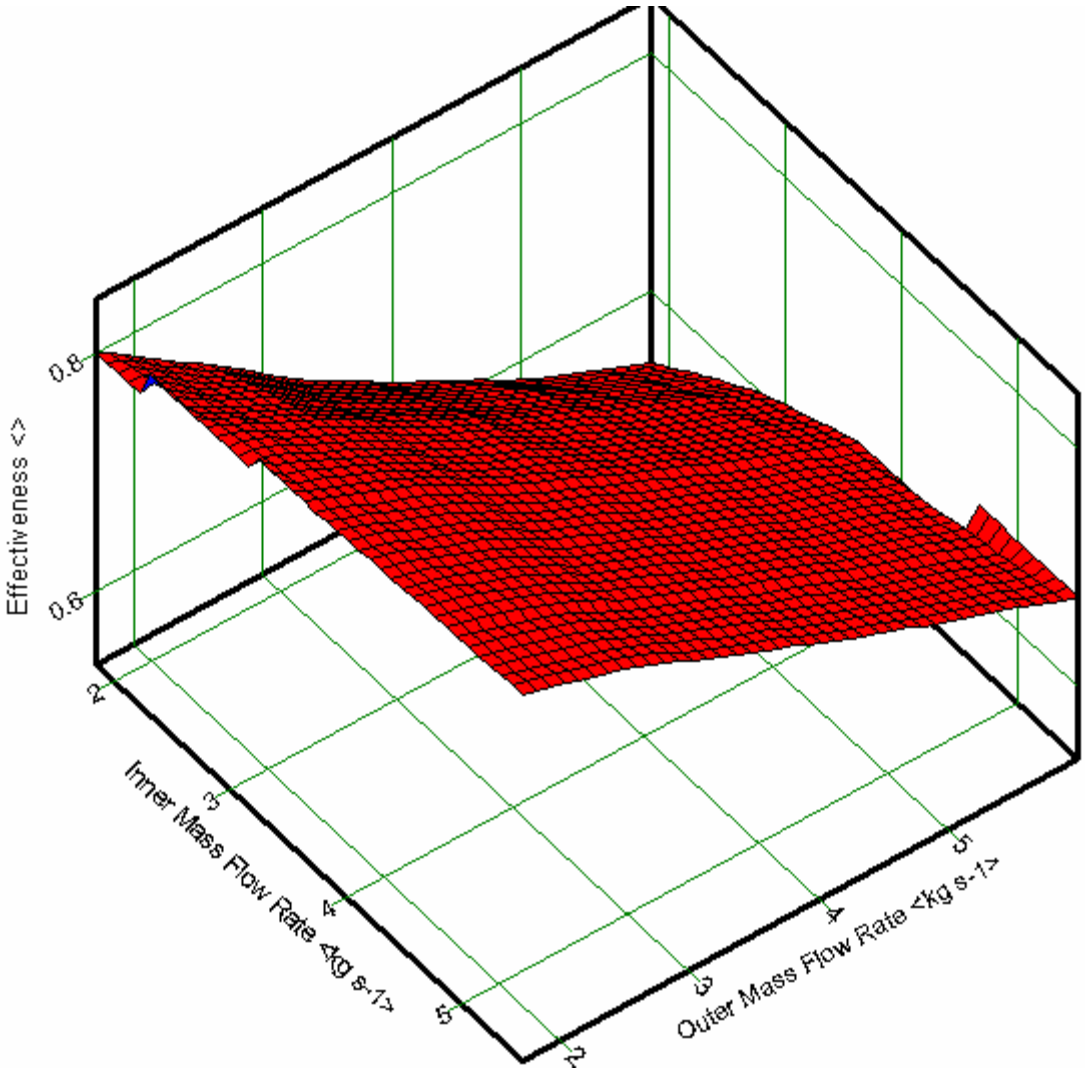

Figure 6. Radiator effectiveness surface plot

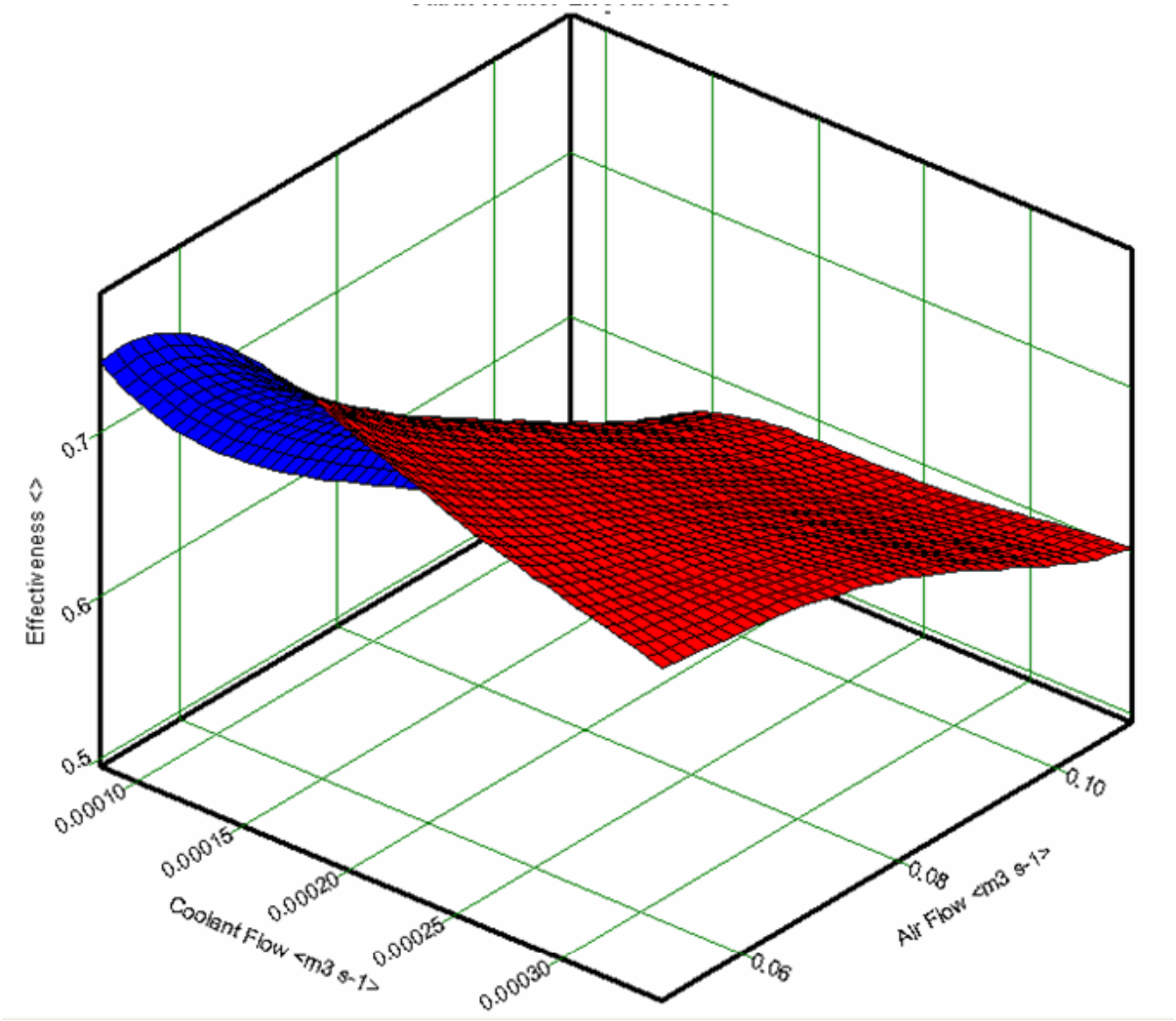

Figure 7. Cabin heater effectiveness surface

The effectiveness for the radiator is improved when using nanofluids as they have enhanced heat transfer coefficients compared with the base fluid. This improvement is evaluated by estimating the overall heat transfer coefficient for the heat exchanger and incorporating the enhanced heat transfer coefficient for the nanofluid on the hot side of the cross-flow heat exchanger. The curves for effectiveness Vs. NTU (Number of Transferred Units) for a cross-flow (unmixed) heat exchanger are used to

Table 4. Radiator effectiveness inputs to FLOWMASTER®

Serial Number	Inner Flow Rate (kg/s)	Outer Flow Rate (kg/s)	Effectiveness (base fluid)	Effectiveness (40% enhanced nanofluid)	Effectiveness (20% enhanced nanofluid)
1	1.84	1.72	0.801465947	0.836481038	0.821526246
2	1.84	2.57	0.740687182	0.786071274	0.766502169
3	1.84	3.42	0.675725467	0.723598572	0.702850719
4	1.84	4.28	0.625015787	0.675534896	0.653525114
5	1.84	5.15	0.576141881	0.626475408	0.604471857
6	1.84	6	0.539100422	0.594774028	0.570236899
7	2.76	1.72	0.824101419	0.851865404	0.840072877
8	2.76	2.57	0.77979434	0.813762039	0.799255611
9	2.76	3.42	0.729086069	0.768201516	0.751404503
10	2.76	4.28	0.680746361	0.721128322	0.703734318
11	2.76	5.14	0.640246638	0.681326083	0.663585698
12	2.76	6	0.599146672	0.644508027	0.624798262
13	3.68	1.71	0.8388171	0.859897801	0.850986742
14	3.68	2.57	0.801604419	0.830680289	0.818312823
15	3.68	3.42	0.753087571	0.786844681	0.77241818
16	3.68	4.26	0.713246693	0.748683249	0.73349877
17	3.68	5.13	0.672420809	0.708917474	0.693239706
18	3.68	6	0.635577912	0.673219082	0.65700648
19	5.51	1.71	0.846656512	0.861566895	0.855290878
20	5.51	2.56	0.820284391	0.842102061	0.832871866
21	5.51	3.43	0.779747218	0.805559925	0.794599765
22	5.51	4.28	0.742624555	0.769991006	0.758346908
23	5.51	5.13	0.708732408	0.736173057	0.72448532
24	5.51	5.99	0.675491651	0.703941217	0.691801023

determine the enhancement in effectiveness for the radiator. This incorporates the enhancement due to nanofluids.

Table 4 shows the difference in effectiveness values for the base fluid and the two nanofluids of this study, for different mass flow rates on both sides. It must be noted that the enhanced effectiveness is calculated for generic nanofluids with 20% and 40% enhancement in heat transfer coefficients and is not specific to CuO based nanofluids.

5. *Thermal bridge*: The thermal bridge models the heat transfer and the pressure drop for the coolant passage through the engine. The heat transfer has been modeled using the Dittus-Boelter Correlation [Dittus and Boelter 1930]. The exponents in the correlation remain the same for the nanofluid but the constant changes corresponding to an enhanced heat-transfer coefficient. The pressure drop is calculated by using a typical loss coefficient for the coolant passages through the engine. The Dittus-Boelter Correlation is given as follows :

$$Nu = a\,(Re)^{b}(Pr)^{c}$$

$$Nu = \text{Nusselt Number} = \frac{hD}{k}$$

$$Re = \text{Reynolds number} = \frac{\rho v D}{\mu}$$

$$Pr = \text{Prandtl number} = \frac{\mu C_p}{k}$$

where *a, b*, and *c* are experimentally determined coefficients.

It has been observed for nanofluids that the exponents for the Reynolds number and the Prandtl number do not show significant deviation from the normal Dittus-Boelter correlation. The constant, a, accounts for the increased heat transfer coefficients of the nanofluids studied. The coefficients for the base fluid and the two nanofluids are given in Table 5.

Table 5. Coolant heat transfer coefficient parameters

Fluid	**Dittus-Boelter Coefficients**		
	a	**b**	**c**
Base Fluid (Ethylene Glycol + Water (50/50))	0.023	0.8	0.4
2% CuO + Glycol/Water (20% enhanced Nu nanofluid)	0.0302731	0.8	0.4
4% CuO + Glycol/Water (40% enhanced Nu nanofluid)	0.038271	0.8	0.4

6. *Discrete loss*: This component is used to model the overall pressure losses in the coolant part of the circuit due to piping, bends etc between the thermostat and the radiator. A generic loss coefficient is used to depict a practical system.

7. *Expansion tank*: The expansion tank is modeled using the 'accumulator' component in the FLOWMASTER code. The accumulator is a closed tank where the coolant is stored. Most expansion tanks are open to the atmosphere. The truck accumulator was modeled as a very large tank, so that it acts as a constant pressure reservoir for the coolant in the circuit similar to the actual system. The pressure of the gas in the accumulator vessel is set to an initial value (approximately equal to the inlet pressure of the coolant at the radiator) to model an actual truck cooling circuit scenario.

2.6 Results

The analysis was first performed for a generic truck engine running at steady state conditions at maximum heat load. The initial set point for the operating conditions is taken as follows:

a) The engine heat rejection to the coolant circuit is 400 hp.

b) The coolant pump is designed for 100 gpm (~ 6 liters/s) at 10 psi (0.68 bars) pressure drop running at 1600RPM.

c) The truck is running at its peak condition of going up a grade (ram air into the radiator comes in at 40 miles/hour) with ambient conditions at 95 ^{0}F (35 ^{0}C).

A pseudo-transient analysis is performed, with interest in the steady state solution for the system. The pseudo-transient analysis helps in arriving at a converged solution for the steady state as the non-linearity like those introduced by thermostat have

significant effect on the convergence. All the simulations have been performed, starting from ambient conditions. The time step is chosen to be 0.5 s and the simulation is run for a total time of 500 s. After a few numerical trials, it was observed that there is no significant change in the thermodynamic properties of the system after about 500 s. In Fig. 8, we show the non-linearity involved in the model due to the presence of the thermostat. The temperature is plotted at the exit of the pump as a function of time.

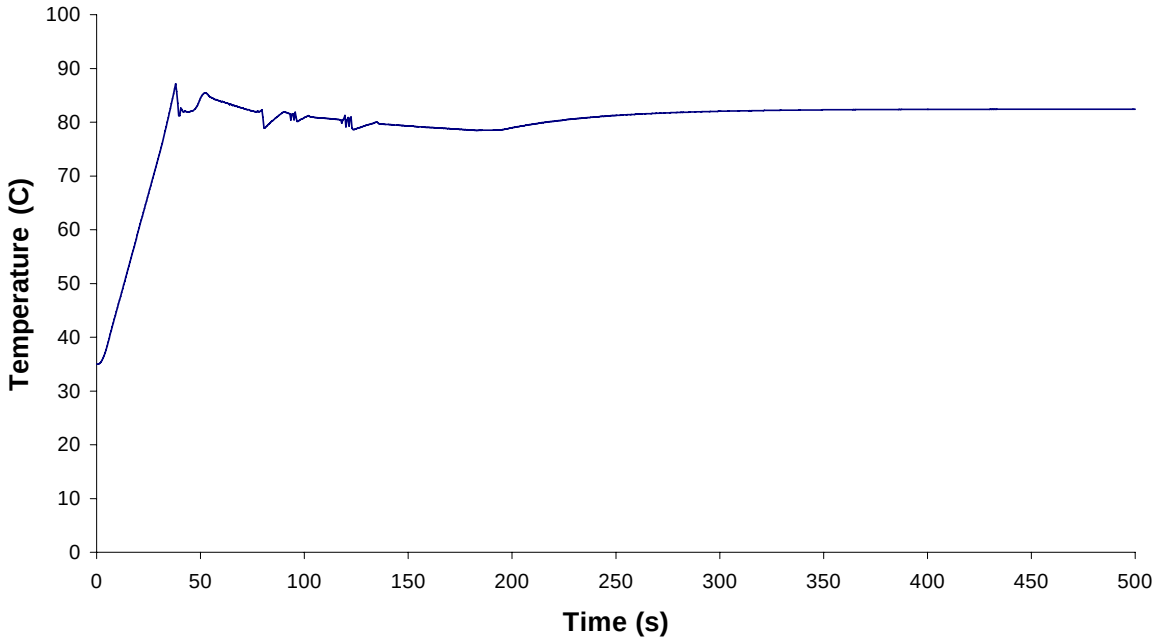

Figure 8. Temperature at exit of pump as a function of time

In Fig. 8, the thermostat opening starts at about 50 s when the temperature of the coolant at the exit of the pump reaches above 80 ^{0}C (approximately). Owing to the difference in pressure drop, between the bypass and the radiator flow paths, there are significant oscillations in temperature of the coolant throughout the system. The above plot also re-

enforces our belief that it reaches a steady state after about 500 s of pseudo-transient analysis.

a) *Base Fluid (Ethylene-glycol + Water (50/50) mixture)*

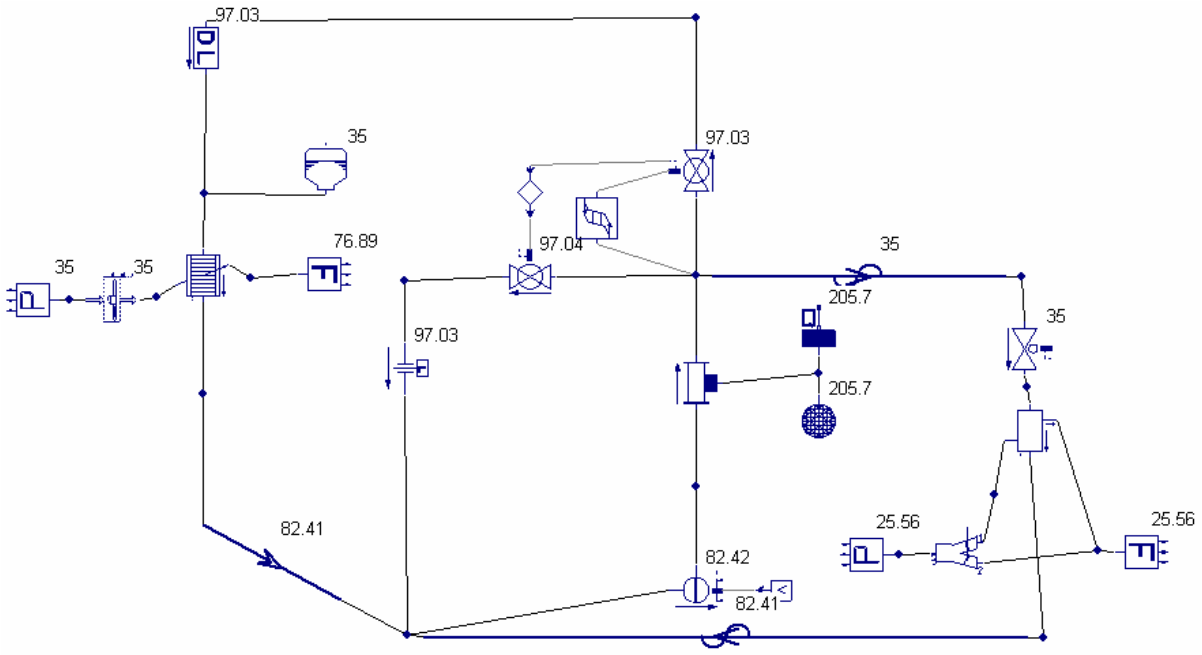

Figure 9. Steady state temperature (^{0}C) distribution (base fluid)

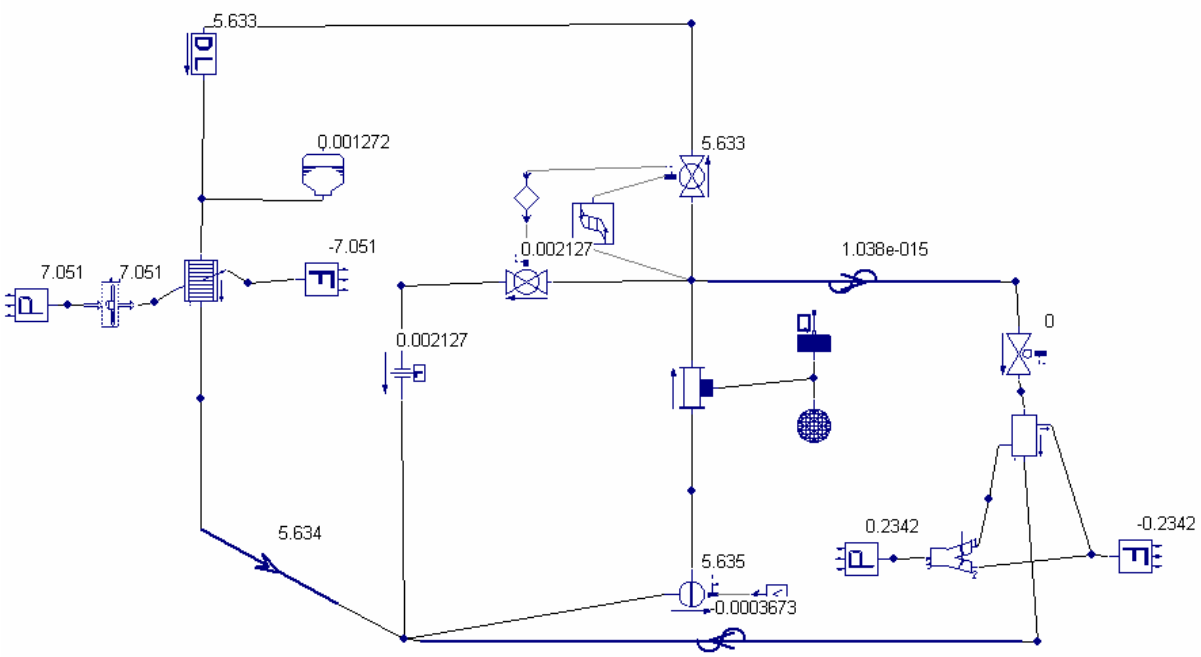

Figure 10. Mass flow rate (kg/s) at steady state (base fluid)

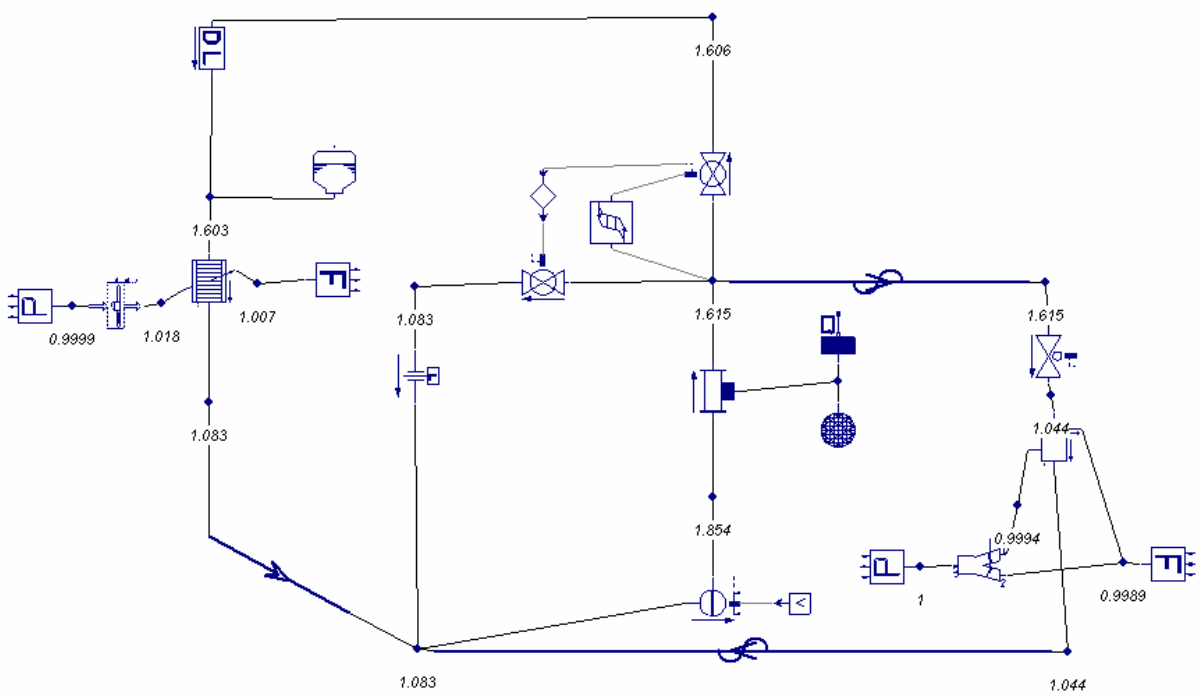

Figure 11. Pressure distribution (bar) at steady state for each node (base fluid)

Figures 9, 10 and 11 show the steady state temperature, mass flow rate and pressure distributions for the working base fluid (ethylene-glycol/water mixture) at various components within the system. Key results include the nominal averaged engine temperature of 206 ^{0}C and the maximum coolant temperature of 97 ^{0}C. Nearly all of the coolant flows (at a mass flow rate of 5.635 kg/s; see Fig. 10) through the radiator with the thermostat fully open and the cabin heater shut-off. The coolant pressure remains below the typical relief pressure of 2 bars (maximum coolant pressure is 1.854 bars; see Fig. 11).

b) *2% CuO nanoparticles by volume in ethylene-glycol/water mixture (nanofluid-1)*

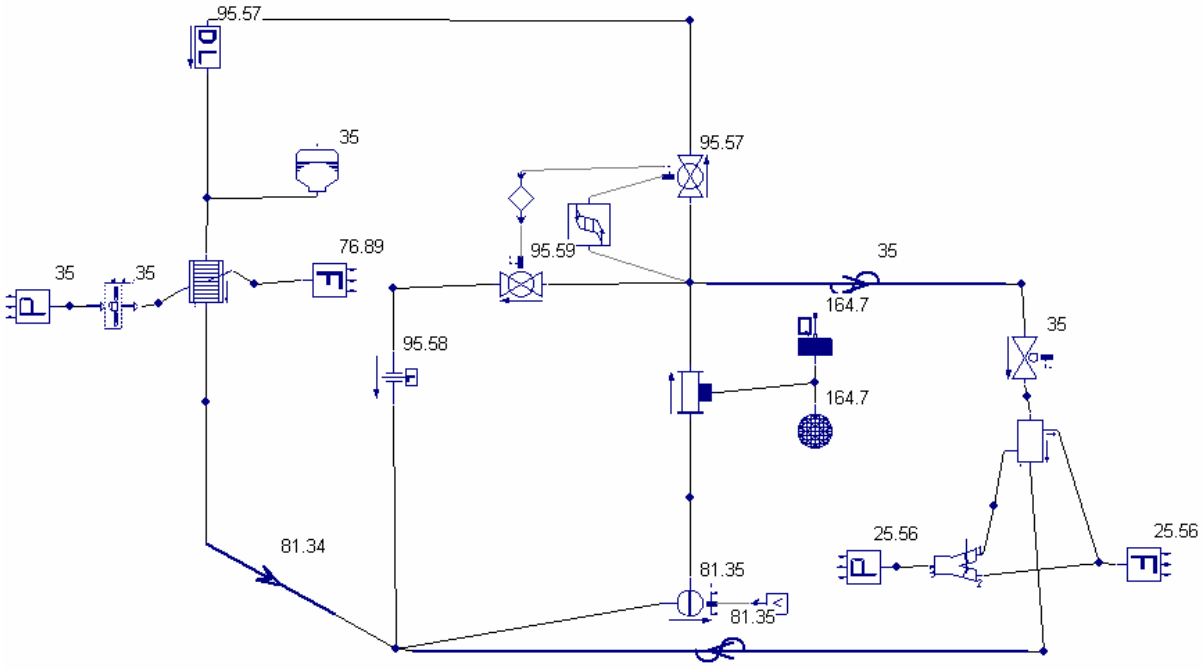

Figure 12. Temperature distribution for base case with nanofluid-1

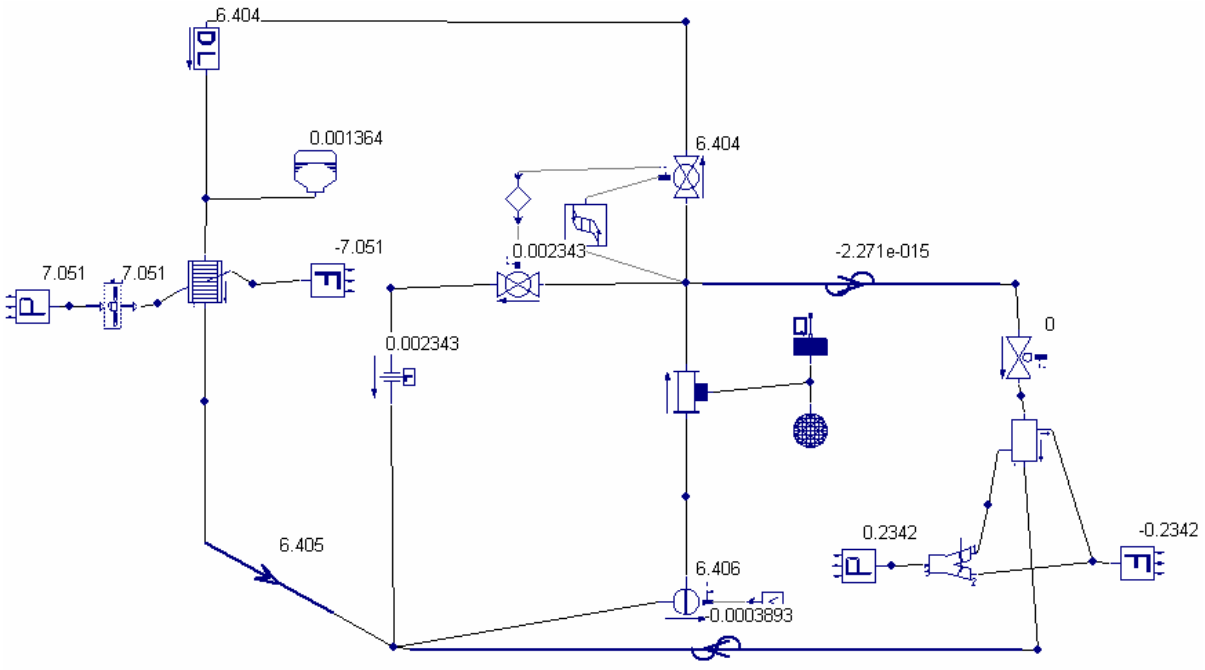

Figure 13. Mass flow rate (kg/s) at steady state for nanofluid-1 (base case)

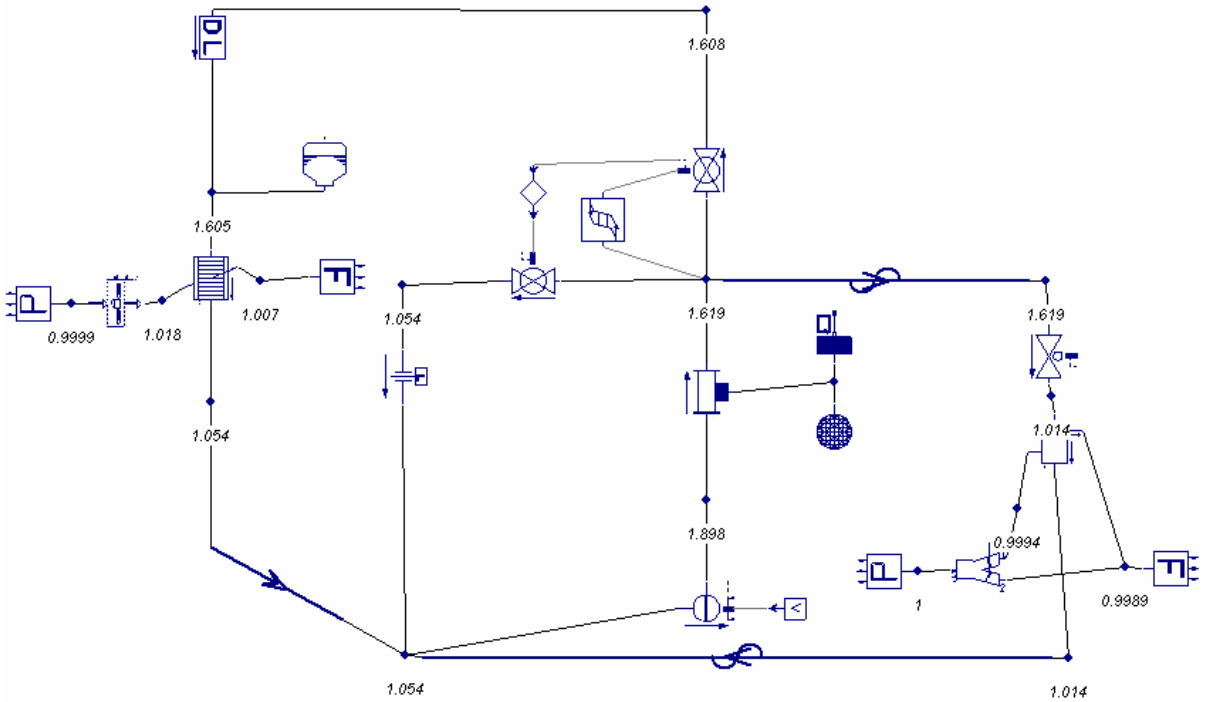

Figure 14. Pressure distribution at nodes for nanofluid-1 (base case)

Replacing the base fluid with a 2% concentration nanofluid in the same engine leads to the results shown in Figs 12-14. Here it can be seen that there is a drop in the maximum temperature attained by the coolant, from 97 ^{0}C to 95.6 ^{0}C. This is due to the increase in effectiveness of the radiator due to the presence of nanofluid in the system. The engine temperature dropped significantly from 206 ^{0}C to 165 ^{0}C and the pressure and flow rate changed only slightly. The engine and coolant temperature changes have important implications for truck coolant system operation and will be discussed further subsequently. The mass flow rate increased from 5.635 kg/s to 6.406 kg/s as compared to the base case owing to the higher density of the nanofluid. There is a slight increase in the maximum pressure within the system from 1.854 to 1.898 bars.

c) *4% CuO nanoparticles by volume in ethylene-glycol/water mixture (nanofluid-2)*

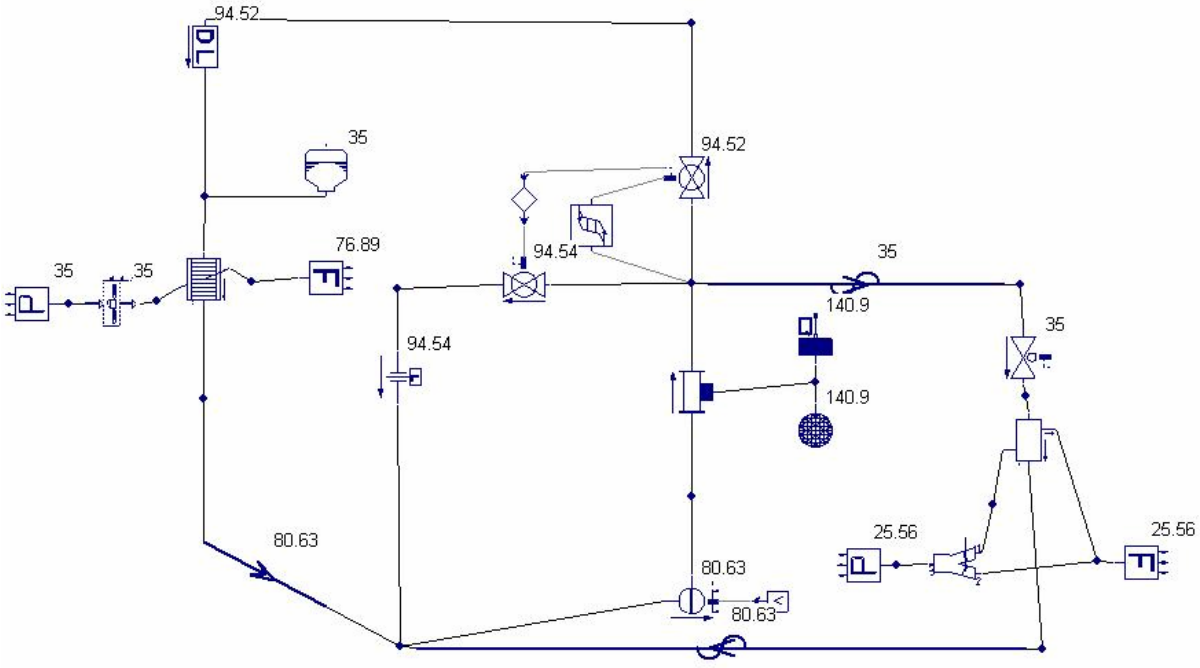

Figure 15. Temperature for base case with nanofluid-2

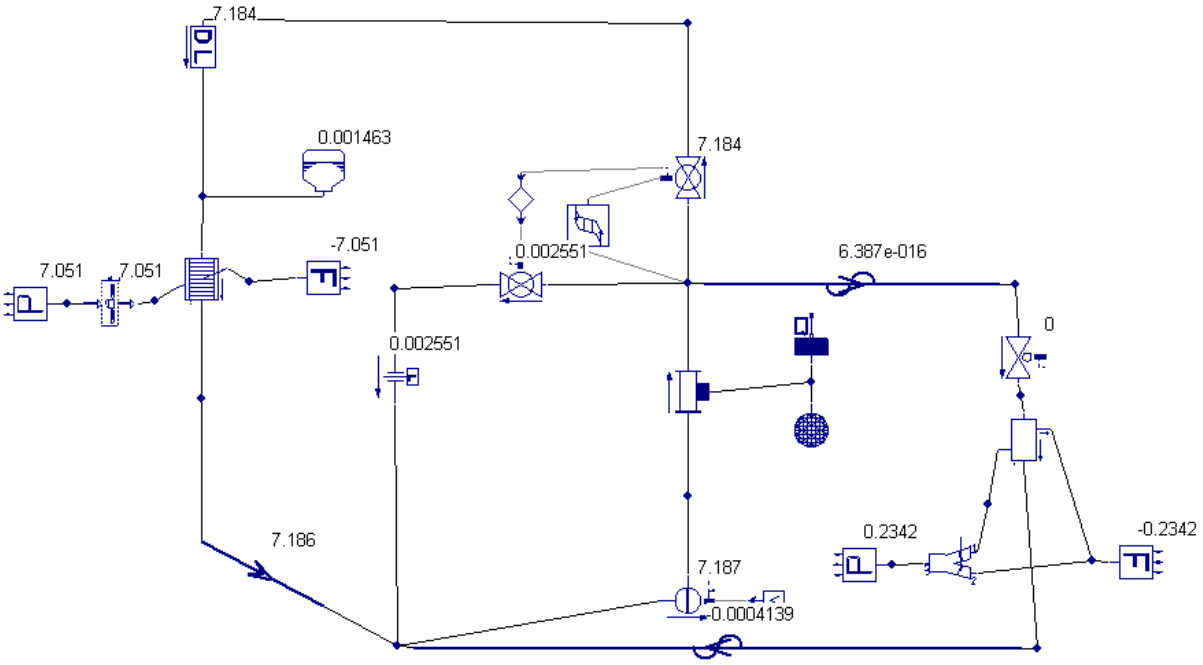

Figure 16. Mass flow rate at steady state with nanofluid-2 (base case)

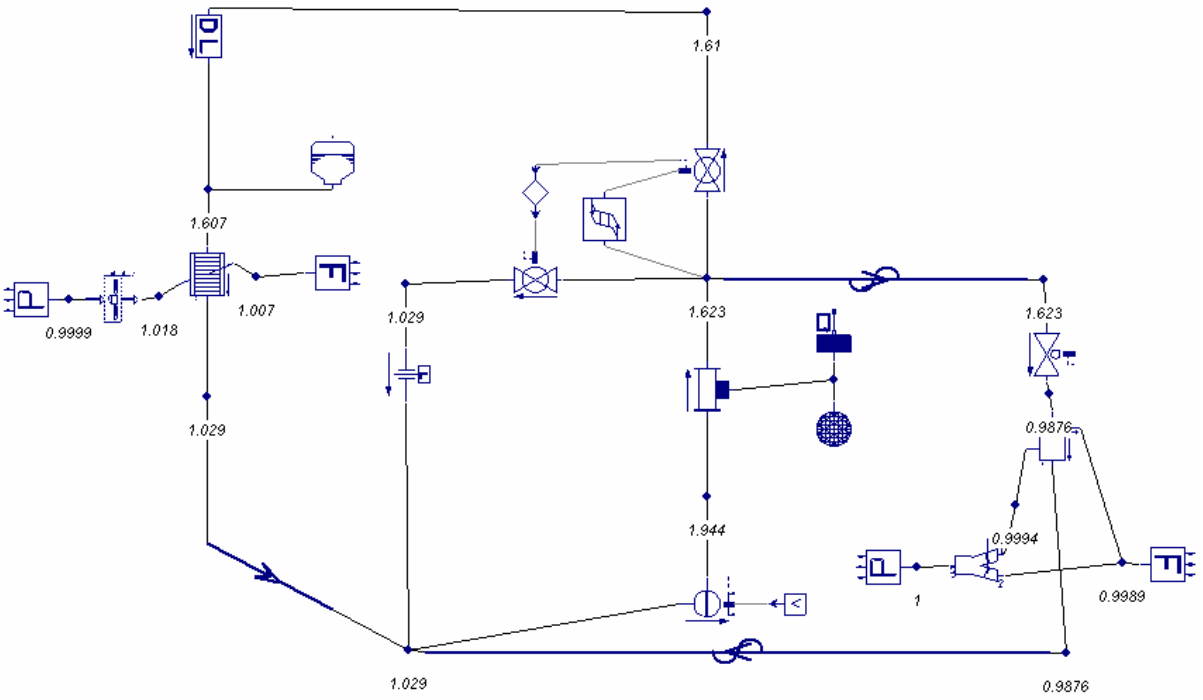

Figure 17. Pressure distribution with nanofluid-2 (base case)

Using a 4% concentration nanofluid in the engine leads to the results shown in Figs. 15-17. This nanofluid is at the upper limit in heat transfer enhancement of what has been reported in the literature using available metal and metal oxide particles. The 40% heat transfer enhancement was used as an upper practical limit of the technology at this time.

The maximum coolant temperature for nanofluid-2 (94.5 ^{0}C) is less than nanofluid-1 (95.6 ^{0}C) which implies higher cooling capabilities with increased concentration. The mass flow rate goes up to 7.187 kg/s compared to the 6.406 kg/s for nanofluid-1 and the original 5.635 kg/s in the base case scenario. The engine temperature is reduced to 141 ^{0}C, and the maximum pressure in the system (1.944 bars) shows only a small change from the base case. It is clear that with higher concentration of particles and higher heat transfer coefficients better cooling of the engine system is achieved. With the improved heat transfer rate with the nanofluids, several options are available for the truck coolant system to optimize its efficiency and performance.

The parameters that can be varied to improve the performance of the system are:

1) Increased maximum engine heat rejection to the coolant circuit (400 hp for base case)
2) Decreased coolant pump RPM and hence power consumption of the pump (1600 RPM for base case)
3) Reduced radiator air-side area (0.39 m^2 for base case)

Numerical simulations were performed for each of the three options listed, and the new systems were designed to keep the maximum coolant temperature the same as that for the base fluid case (~ 97 ^{0}C).

2.6.1 Increasing engine heat rejection

a) *Nanofluid-1*

From the numerical simulation results, it was observed that an engine heat rejection of 410 hp (305.87 kW) would be attainable for other conditions remaining the same and replacing the coolant with a nanofluid containing 2% CuO nanoparticles. Details are given in Figures 18-20. In Fig. 19, it can be observed that there is about 19% increase in mass flow rate as compared to the base case (with base fluid) mass flow rate. The pressure distribution (shown in Fig. 20) remains the same as compared to the pressure distribution for the scenario replacing the base fluid with the nanofluid (as shown in Fig. 14).

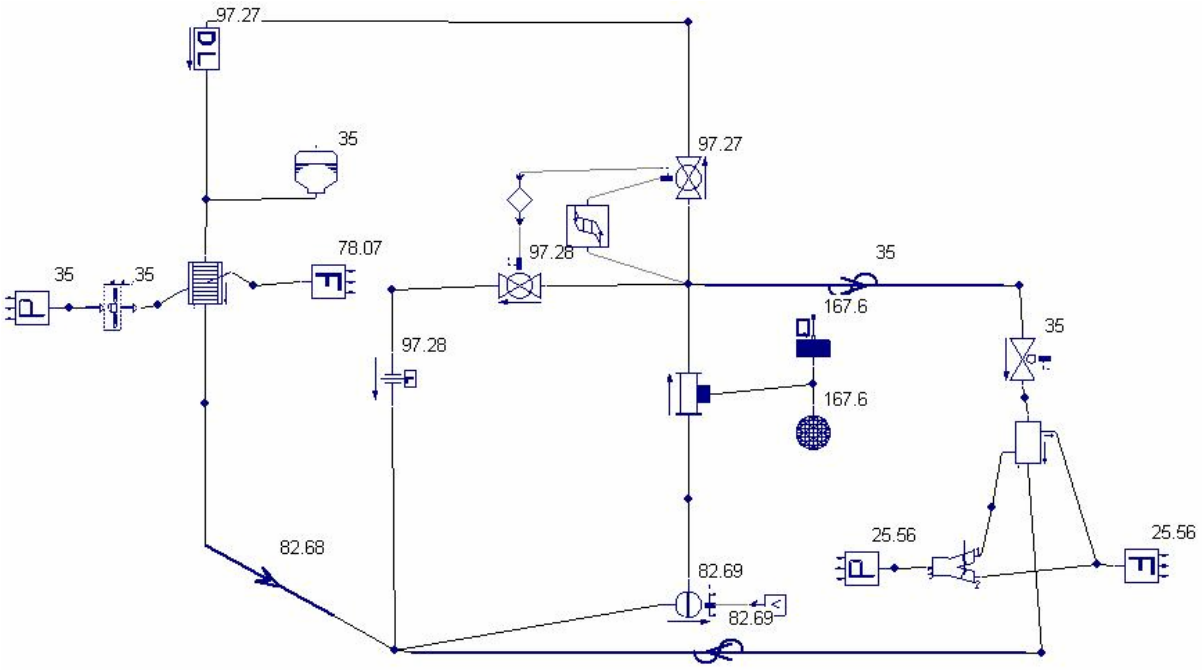

Figure 18. Temperature at 410 hp engine heat rejection (nanofluid -1)

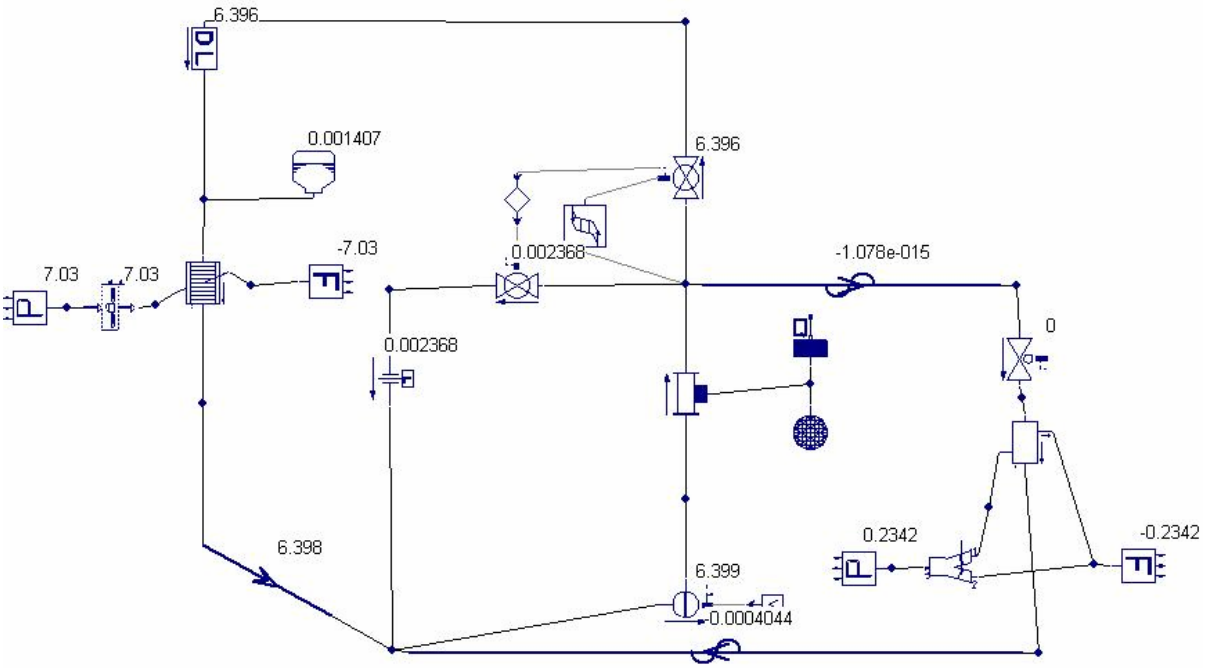

Figure 19. Mass flow rate at 410 hp engine heat rejection (nanofluid -1)

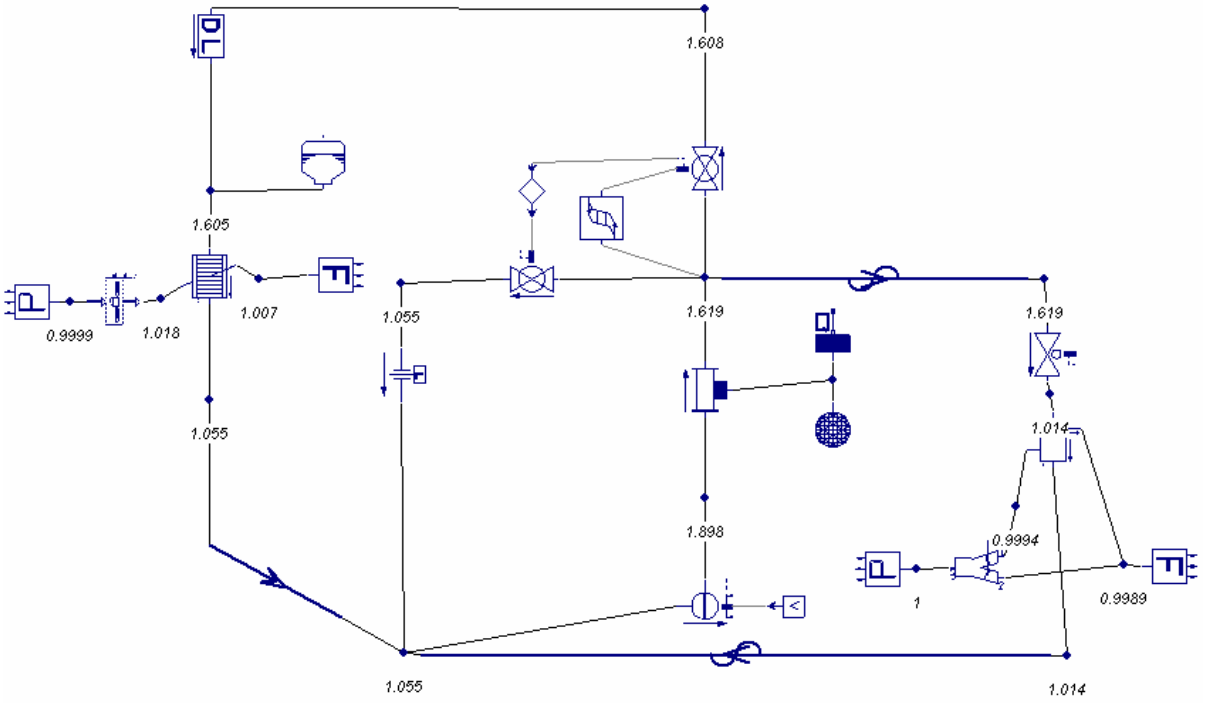

Figure 20. Pressure dirstribution at 410 hp engine heat rejection (nanofluid -1)

b) *Nanofluid-2*

For a higher concentration, up to 420 hp (313.32 kW) of engine heat can be rejected to the coolant circuit and the coolant temperature can be kept within desirable limits as shown in Fig. 21. The coolant flow and pressure are given for this case in Fig. 22 and 23, respectively. As observed for nanofluid-1, the pressure distribution remains almost the same (Figs. 11 and 23) whereas the mass flow rate goes up to 7.172 kg/s from 5.635 kg/s in the base case showing about 27% increase (Figs. 10 and 22) .

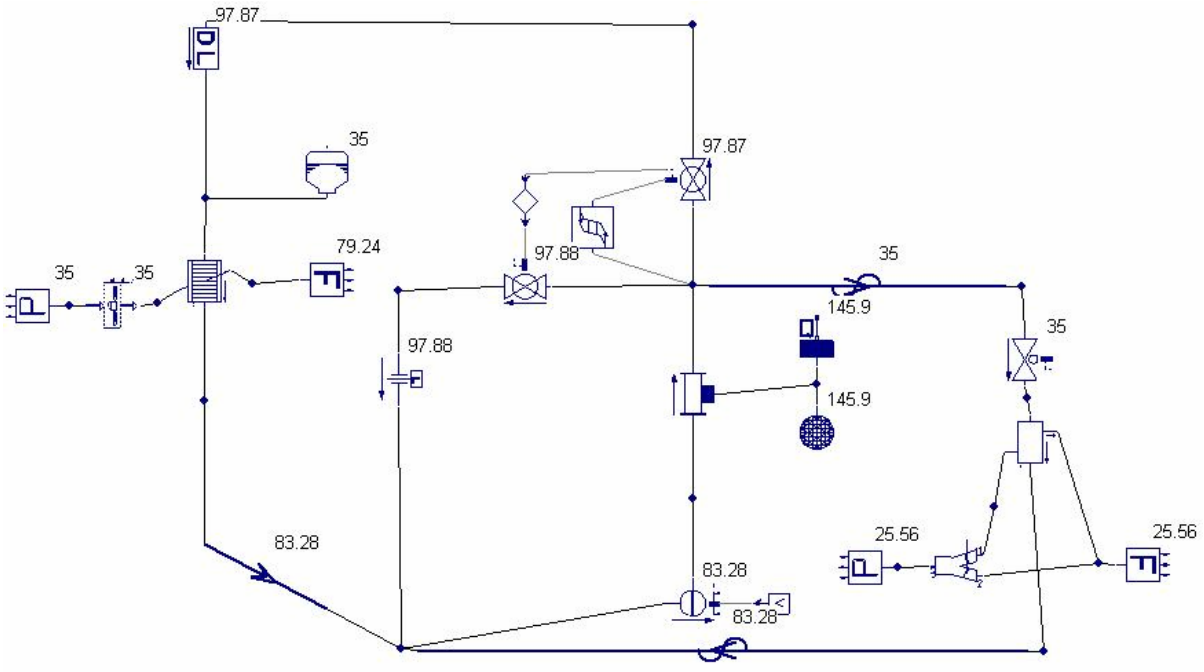

Figure 21. Temperature distribution at 420 hp engine heat rejection (nanofluid -2)

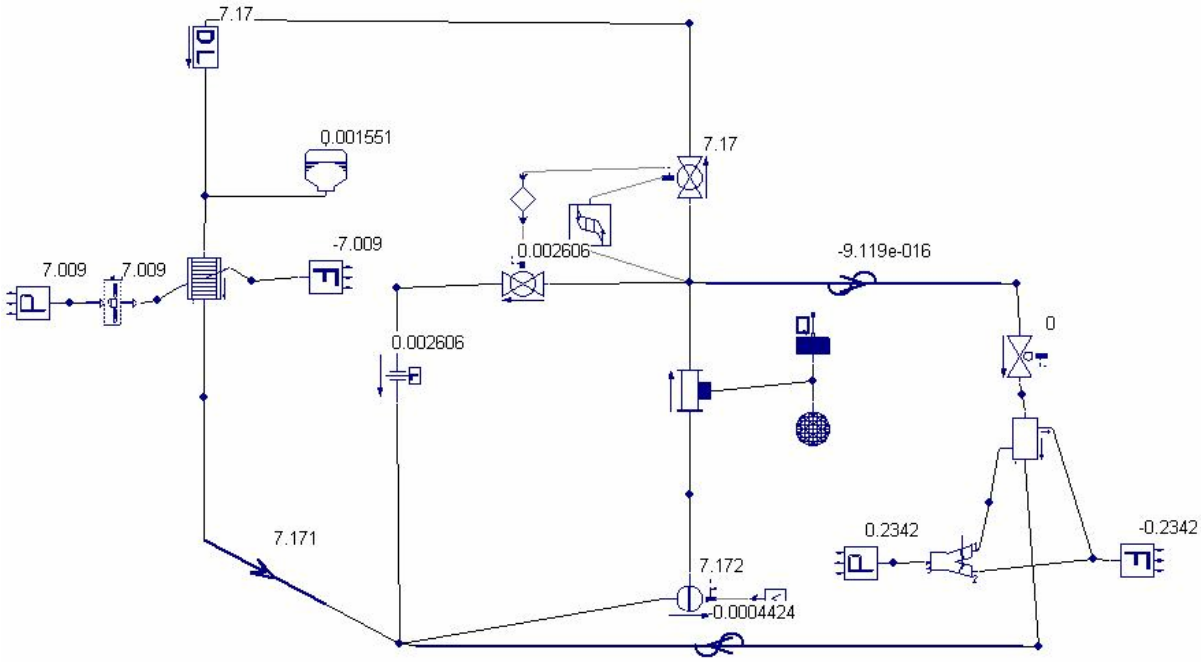

Figure 22. Mass flow rate at 420 hp engine heat rejection (nanofluid -2)

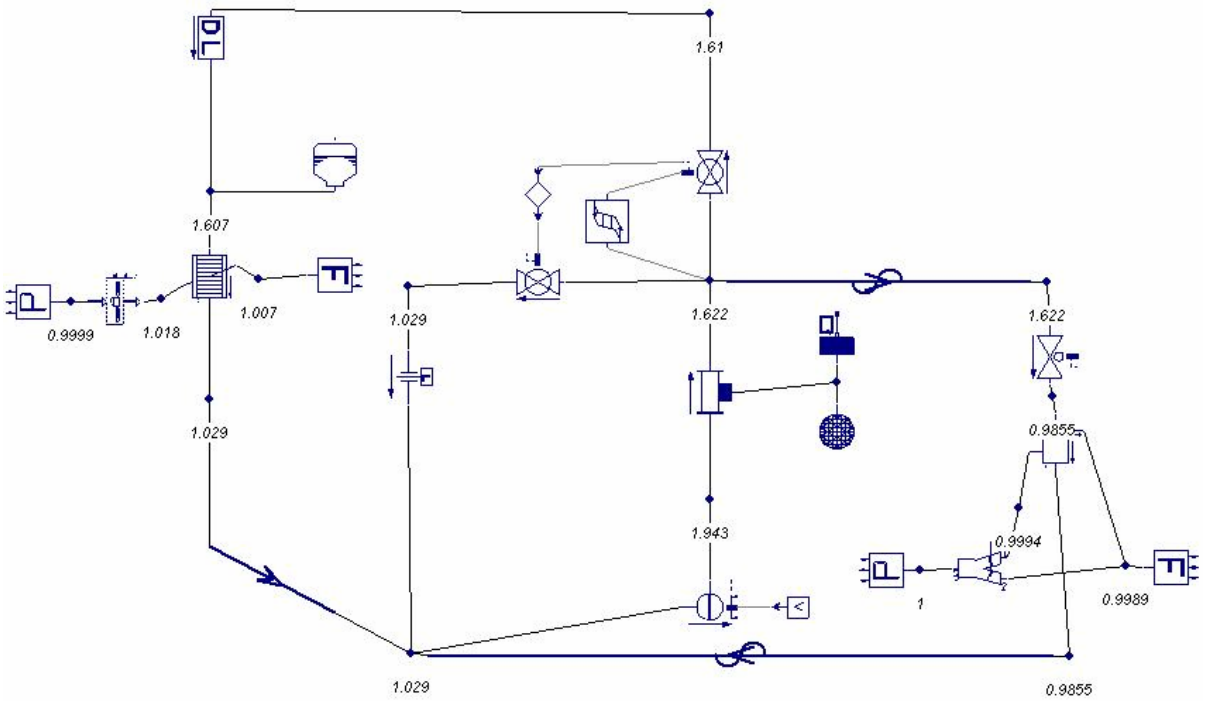

Figure 23. Pressure distribution at 420 hp engine heat rejection (nanofluid -2)

2.6.2 Decreasing coolant pump speed

a) *Nanofluid-1*

The pump speed can be reduced significantly. For nanofluid-1, the pump speed can be reduced from 1600 RPM (base case) to about 1150 RPM and still have the coolant temperature below the maximum limit as shown in Figure 24. The coolant flow rate (Figure 25) reduces to about 4.616 kg/s which is approximately 20% reduction in mass flow rate. The maximum pressure in the circuit reduces to 1.75 bars (compared to 1.85 bars in base case; see Fig. 11) which is desirable owing to overall safety of the closed loop system as shown in Fig. 26.

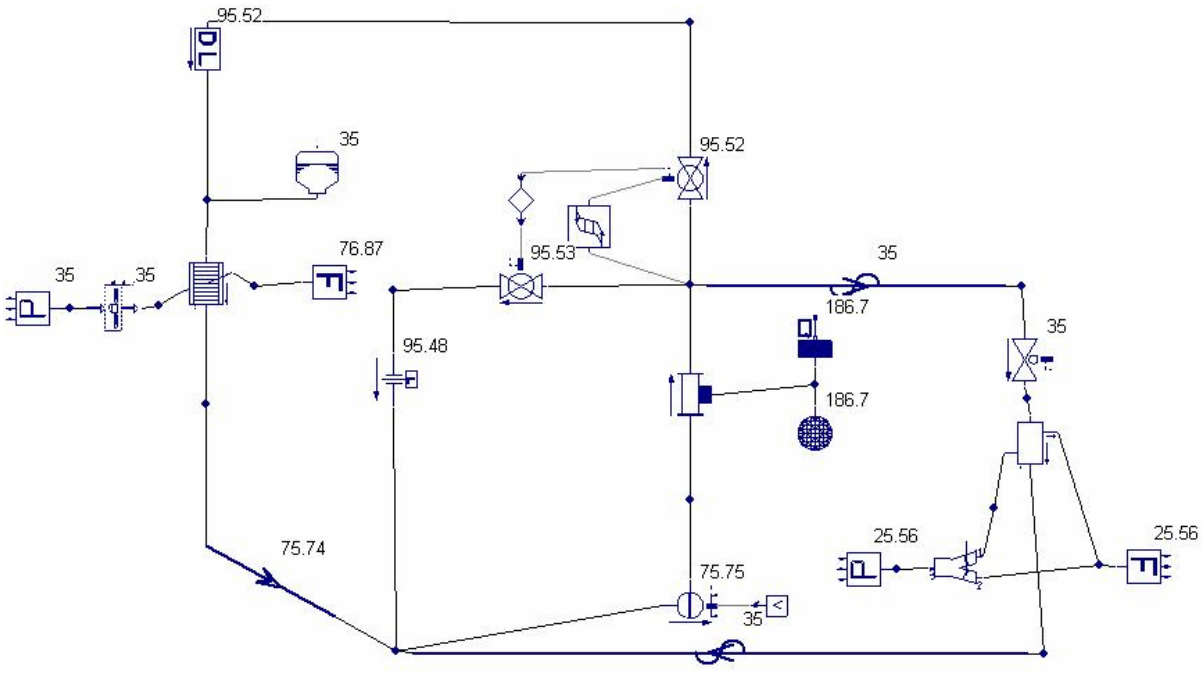

Figure 24. Temperature at 1150 RPM (nanofluid -1)

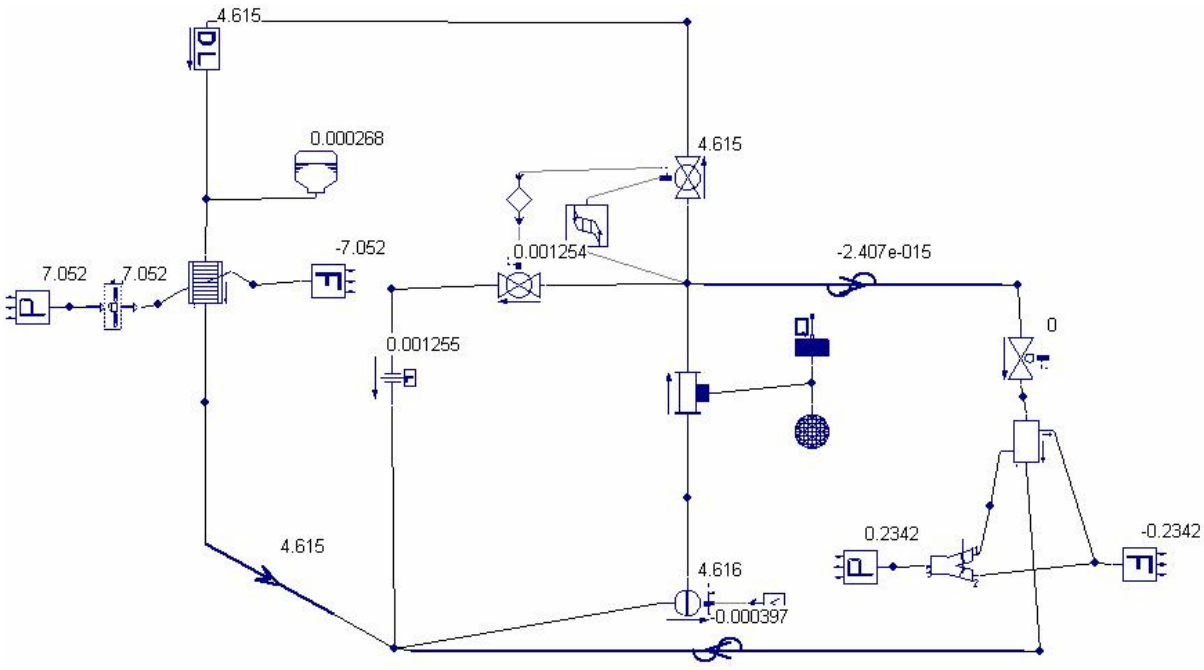

Figure 25. Mass flow rate at 1150 RPM (nanofluid -1)

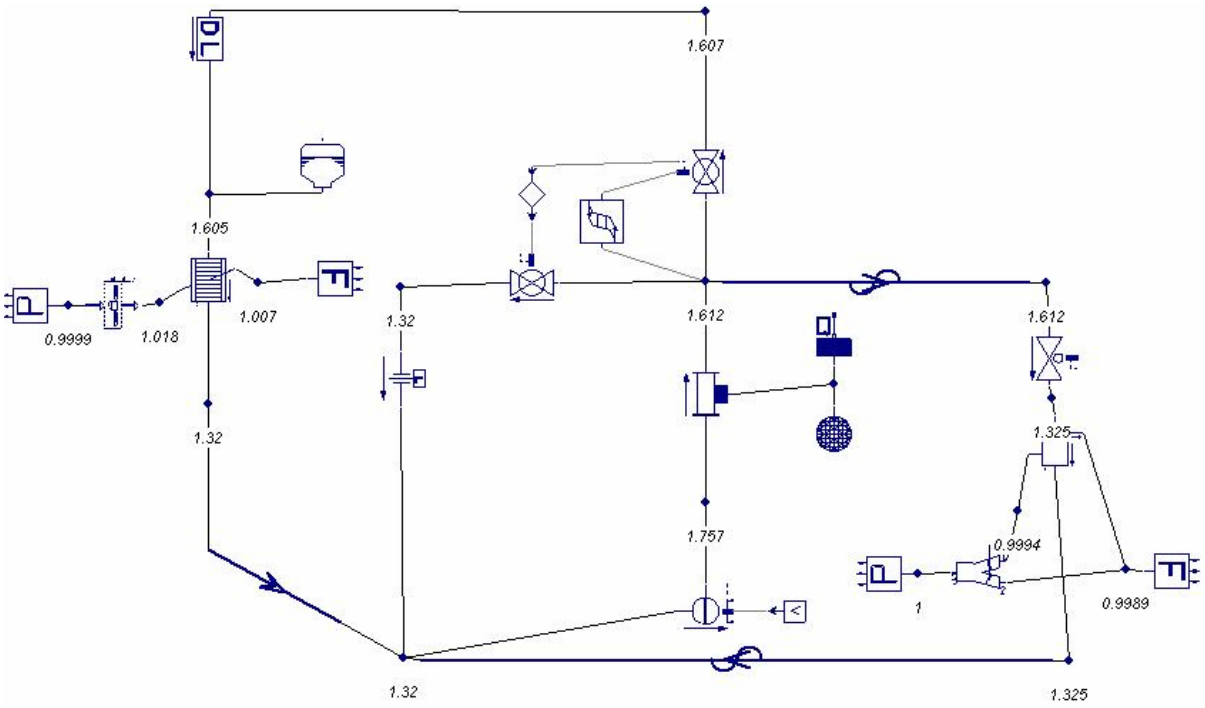

Figure 26. Pressure at 1150 RPM (nanofluid -1)

The reduction of pump speed from 1600 RPM to 1150 RPM brings about a reduction of pump power consumption from 0.56 kW (0.75 HP) to about 0.2 kW (0.266 HP).

b) *Nanofluid-2*

The nanofluid-2 has an even better impact on the pump power. The reduction in speed also implies lower pressure losses (maximum pressure being about 1.69 bar as seen in Fig. 27 compared to 1.85 bar in base case as seen in Fig. 11) due to lower flow-rates, hence enhanced efficiency. For this case, the pump speed can be reduced to 800 RPM while maintaining the maximum limit on the coolant temperature. The mass flow rate drops down to 3.625 kg/s compared to 5.635 kg/s in the base case

which is about 35% reduction in overall mass flow. The details are shown in Figs. 27-29.

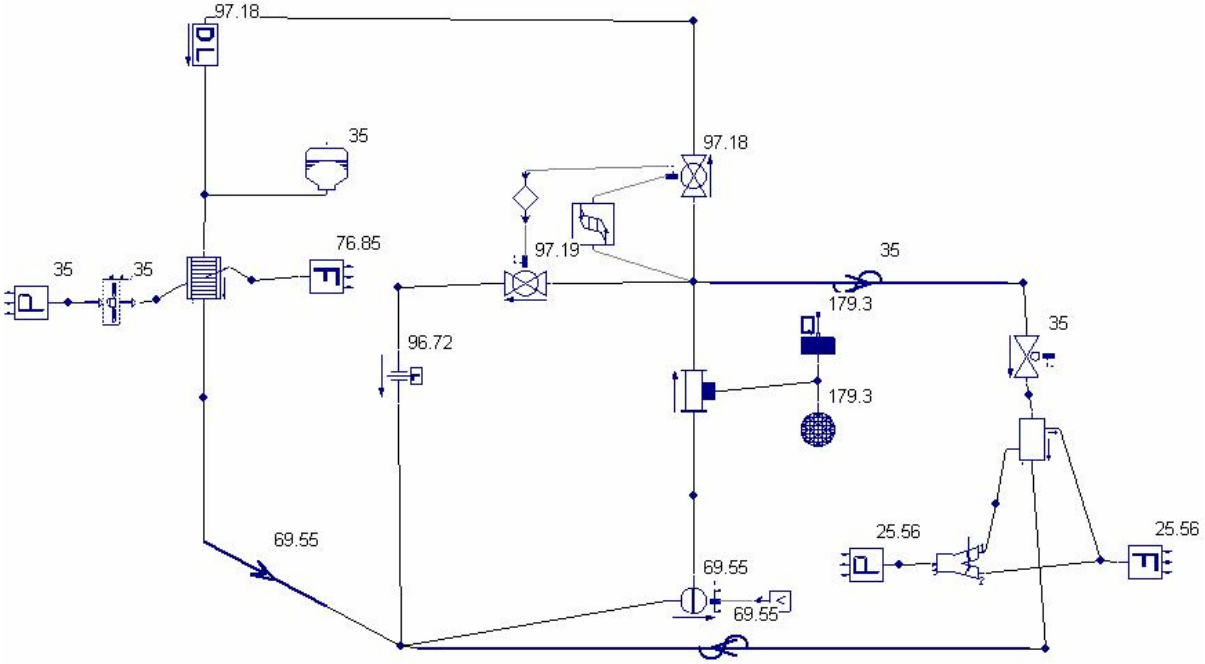

Figure 27. Temperature distribution at 800 RPM (nanofluid -2)

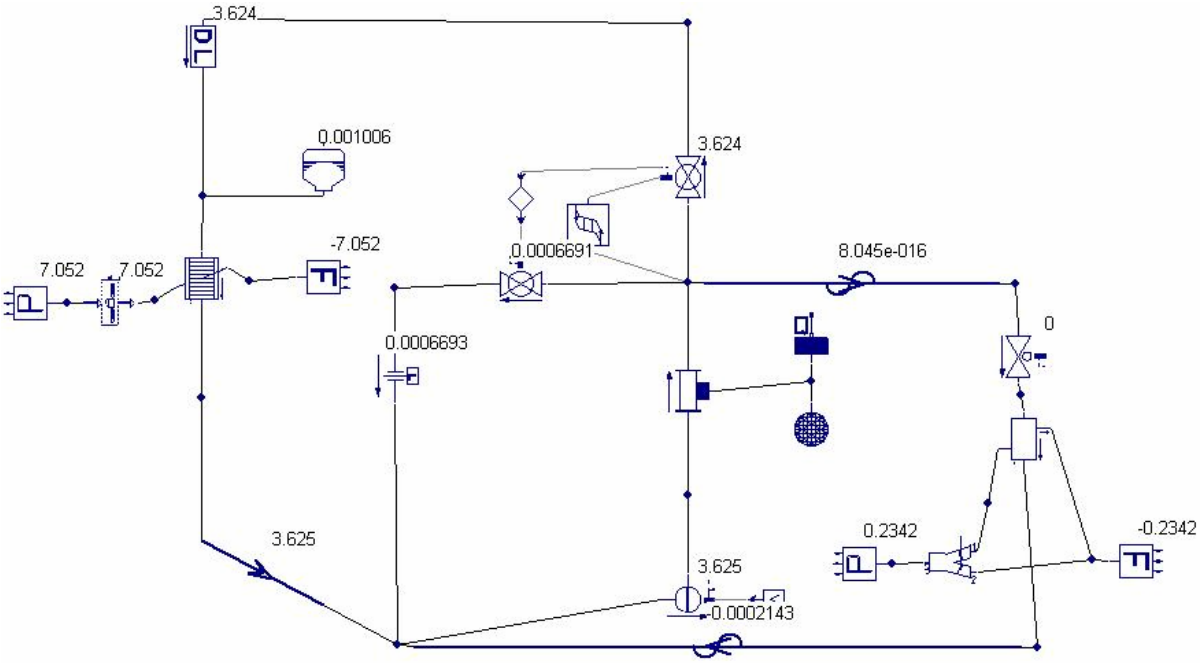

Figure 28. Mass flow rate at 800 RPM (nanofluid -2)

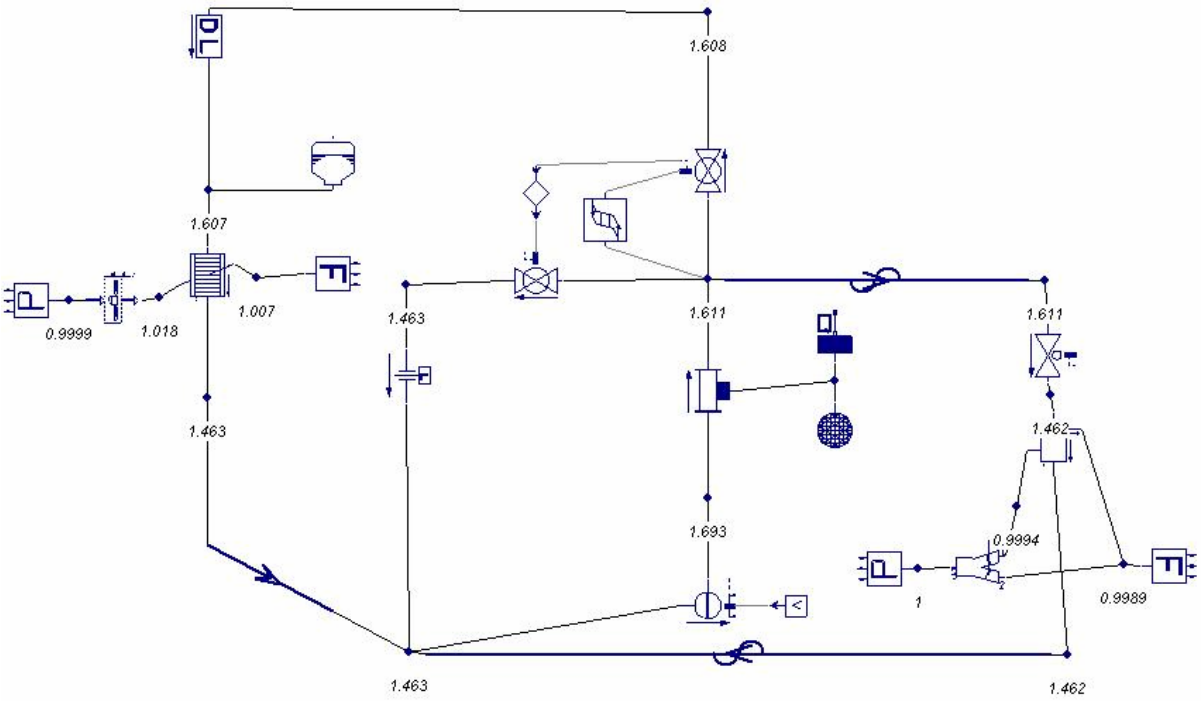

Figure 29. Pressure distribution at 800 RPM (nanofluid -2)

For nanofluid-2, the pump consumes only 0.0675 kW of power as compared to 0.56 kW of power for the base case. This is expected since power consumption varies as the cube of the pump rpm. This is almost an order of magnitude reduction in pump power. Such low power consumption is amenable to an electric drive which can be optimized for performance and efficiency. This is a significant contrast to the current coolant pumps that are mechanically belt driven based on the engine speed.

2.6.3 Radiator air-side area reduction

The final parametric study involved the reduction in air-side radiator flow area and hence the reduction of the flow rate of air over the radiator.

a) Nanofluid-1

The air-side area can be reduced to 0.38 m^2 from 0.39 m^2. Though this seems to be a small number, the fact that has to be kept in mind is that the truck is simulated for the worst case scenario and that the overall heat transfer coefficient is dominated by the air-side on the radiator. Hence, significant enhancements are not expected by improving the hot-side coolant properties of the radiator. Results of this case are shown in Figs. 30-32. The performance is optimized taking the maximum coolant temperature (~ 97.3 ^{0}C) into consideration. The mass flow rate shows a 13.5% increase as compared to the base flow scenario (~ 5.633kg/s) whereas the pressure distribution remains almost the same with maximum pressure being 1.898 bars.

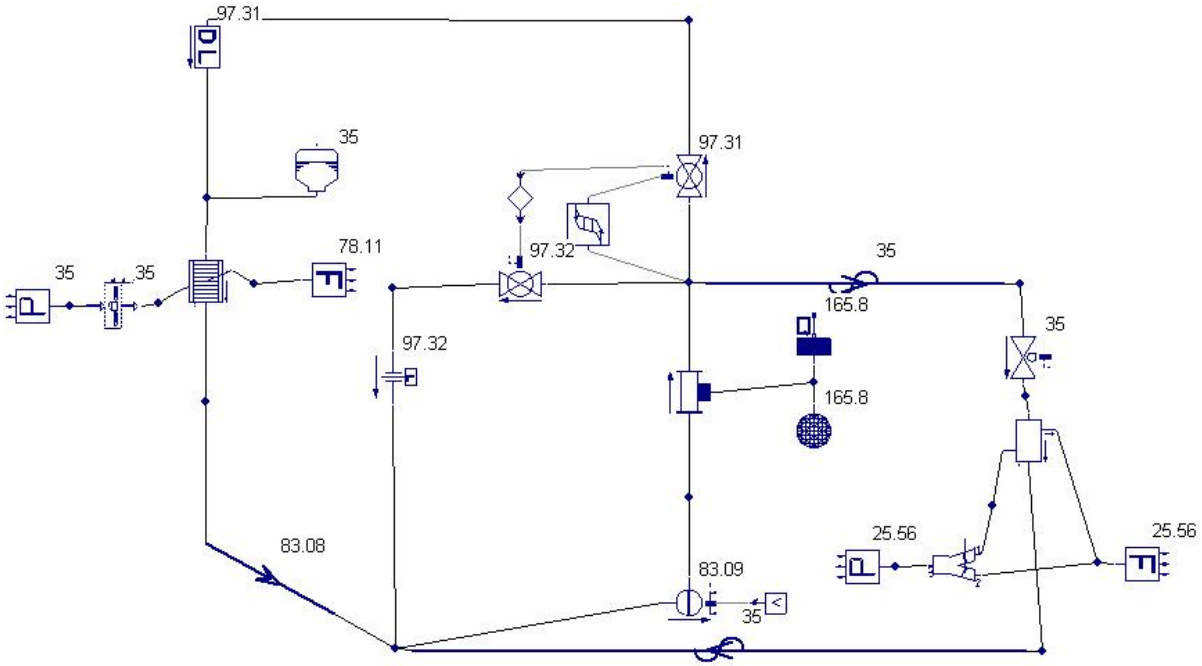

Figure 30. Temperature distribution for 0.38 m^2 radiator air-side area (nanofluid -1)

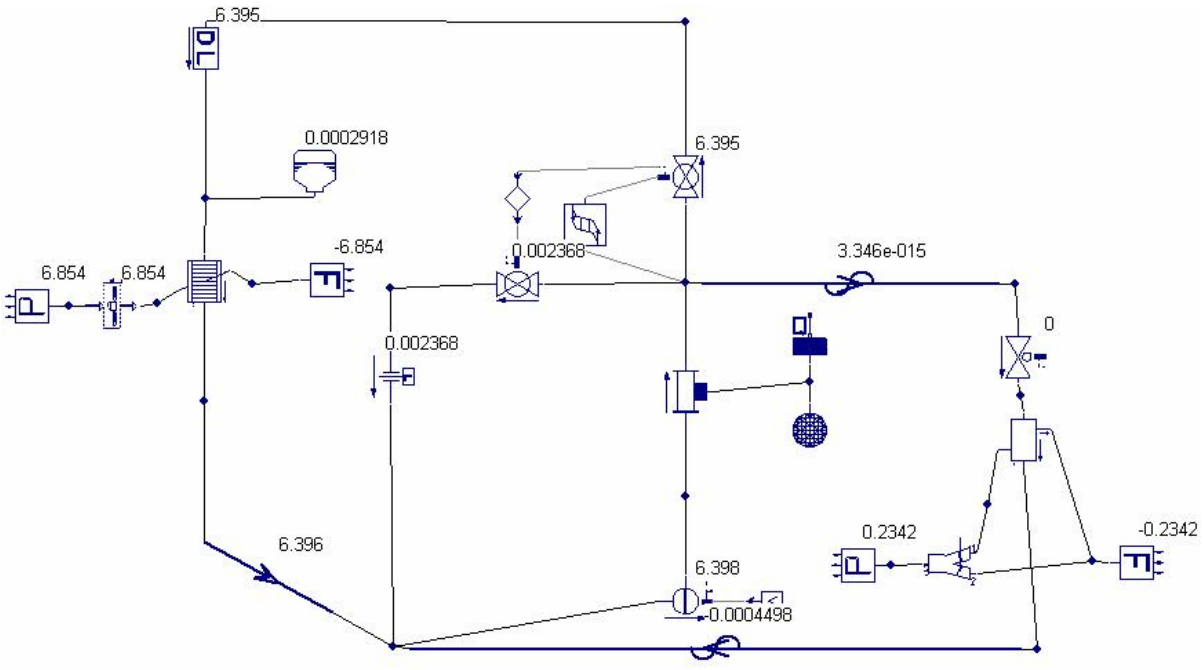

Figure 31. Mass flow rate for 0.38 m^2 radiator air-side area (nanofluid -1)

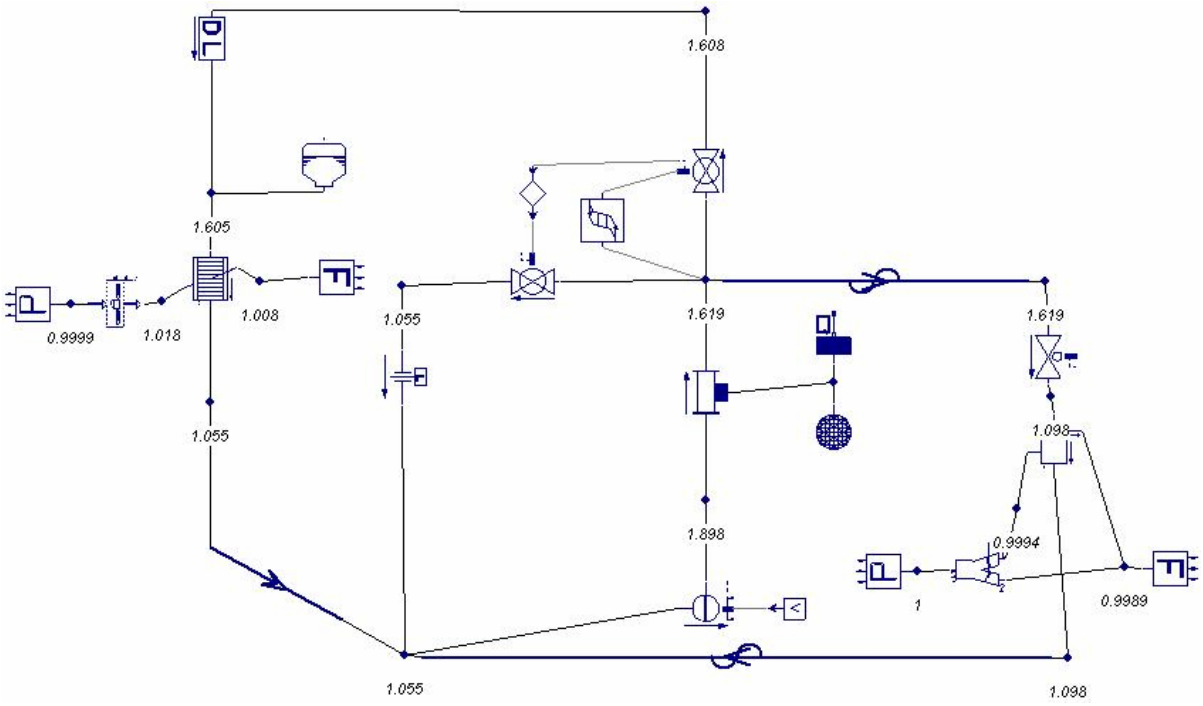

Figure 32. Pressure distribution for 0.38 m^2 radiator air-side area (nanofluid -1)

b) Nanofluid-2

For nanofluid-2, the air-side area can be reduced to 0.37 m^2 from the original value of 0.39 m^2. This is 5.13% decrease in the radiator air-side area. As in the previous case, the optimization is again based on maximum coolant temperature (~ 98 ^{0}C; see Fig. 33). The mass flow rate shows a marked increase of approximately 27% (see Fig. 34) whereas the maximum pressure (~ 1.898 bars; see Fig. 35) shows a small change compared to the base case flow and pressure distribution scenarios. In general, a 5% reduction in truck frontal area can be used to reduce the aerodynamic drag and to increase the fuel efficiency by 2.5%. This level is significant for the "Class 8" truck that averages about 6 miles per gallon of gasoline consumption.

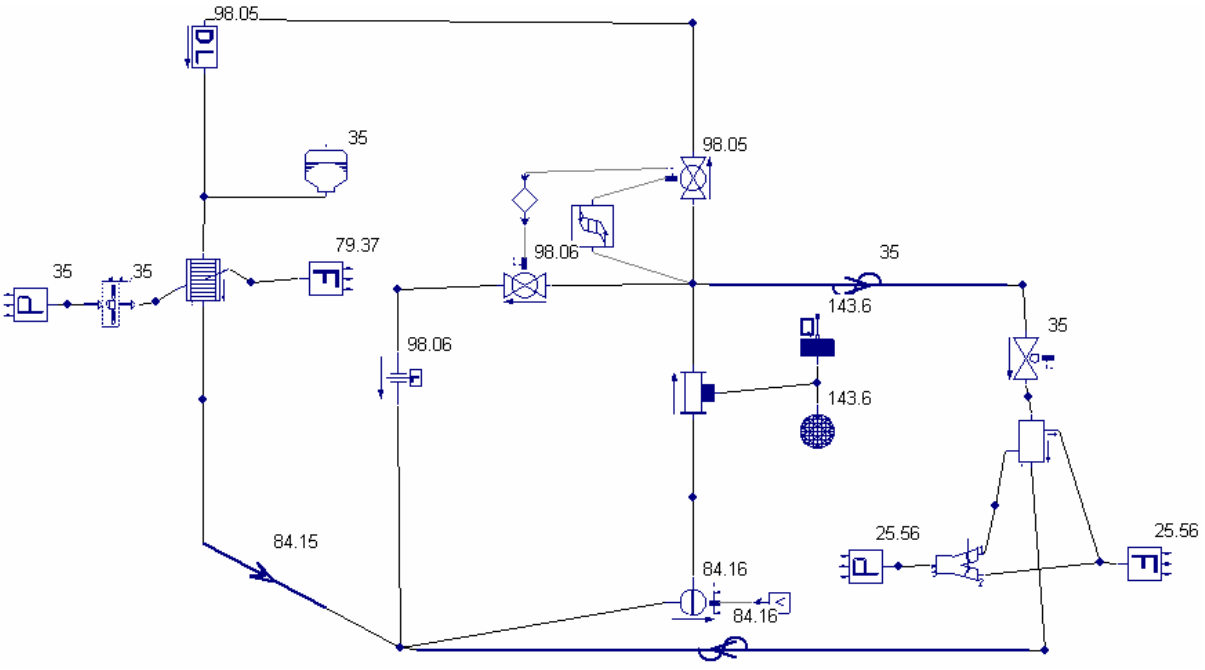

Figure 33. Temperature distribution for 0.37 m^2 radiator air-side area (nanofluid -2)

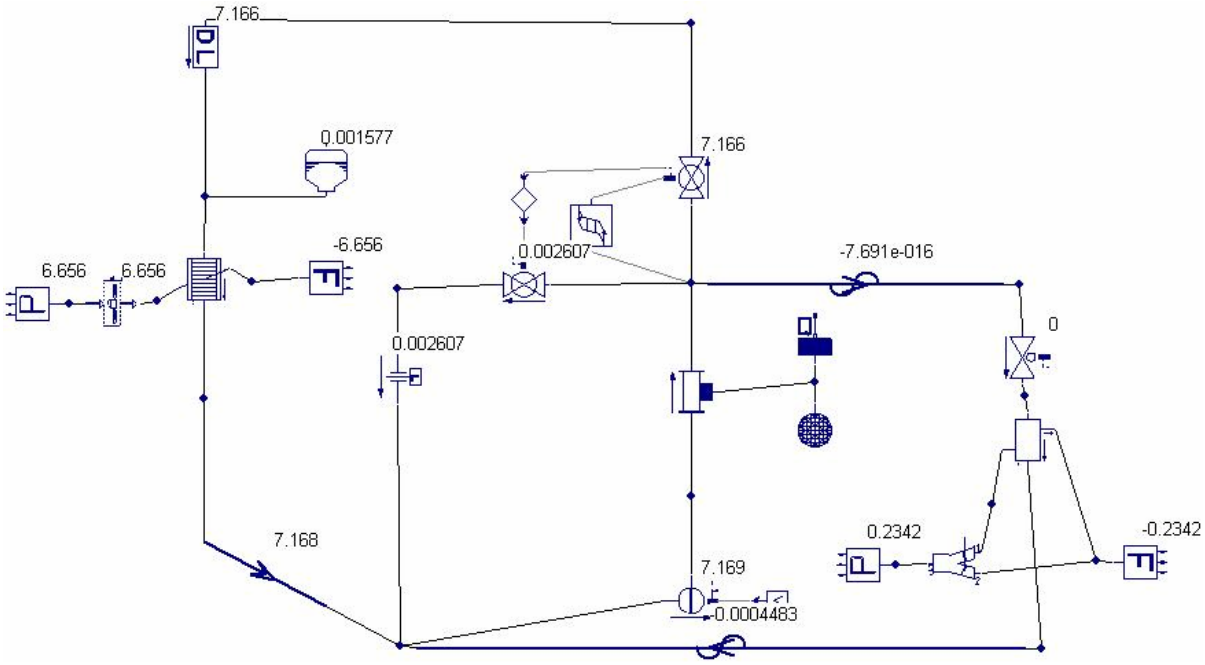

Figure 34. Mass flow rate for 0.37 m^2 radiator air-side area (nanofluid -2)

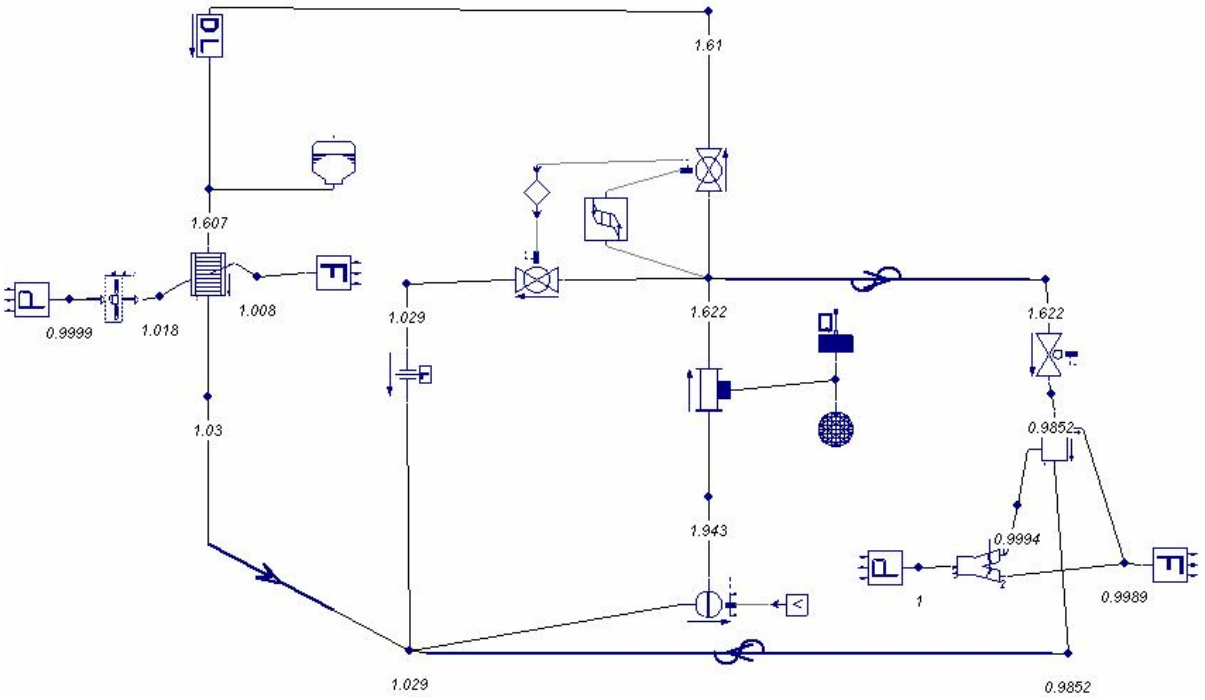

Figure 35. Pressure distribution for 0.37 m^2 radiator air-side area (nanofluid -2)

2.7 Comparison of results

The results are compared for all the 3 parametric study cases.

a) *Engine heat rejection*

The maximum engine heat rejection to coolant increases steadily as the concentration of nanoparticles in the base fluid increases. The increase is not the same order of magnitude as the increase in conductivity or heat transfer coefficient. About 5% increase in heat rejection may be expected, as shown below.

Table 6. Comparison of increase in engine heat rejection between base fluid and nanofluids

Serial No.	Fluid	Maximum Engine Heat Rejection to Coolant Circuit
1	Base Fluid (ethylene-glycol/water (50/50) mixture)	400 hp (298.4 kW)
2	2% CuO nanoparticles by volume in ethylene-glycol/water mixture	410 hp (305.86 kW)
3	4% CuO nanoparticles by volume in ethylene-glycol/water mixture	420 hp (313.32 kW)

b) *Radiator air-side area*

The radiator air-side area is an important factor for the truck design. For this case, it was observed that the air-side area decreases as the particle concentration increases. The effect on the air-side area is not dominant owing to the fact that the overall heat transfer coefficient is dominated by the air-side of the radiator. Hence, a significant increase in the heat transfer coefficient on the coolant-side would not have a very significant impact on the air side. Maximum reduction of about 5% is observed in this parameter keeping all other conditions being kept the same.

Table 7. Reduction of air-side area for nanofluids compared to base fluid

Serial No.	Fluid	Radiator air-side area
1	Base Fluid (ethylene-glycol/water (50/50) mixture)	0.39 m^2
2	2% CuO nanoparticles by volume in ethylene-glycol/water mixture	0.38 m^2
3	4% CuO nanoparticles by volume in ethylene-glycol/water mixture	0.37 m^2

c) *Coolant pump speed (RPM)*

A significant reduction in the coolant pump power and the flow rate can be achieved by replacing the conventional coolant by a nanofluid. The results are summarized in Table 8 below.

Table 8. Reduction of coolant pump power and speed for nanofluids compared to base fluid

Serial No.	Fluid	Pump Speed (RPM)	Pump Power (kW)
1	Base Fluid (ethylene-glycol/water (50/50) mixture)	1600	0.52
2	2% CuO nanoparticles by volume in ethylene-glycol/water mixture	1150	0.2
3	4% CuO nanoparticles by volume in ethylene-glycol/water mixture	800	0.0675

This also implies a much lower mass flow rate of coolant to maintain the same maximum temperature. Though the absolute decrease in pump power is not large, the percentage decrease is still significant. The pump power can be reduced by approximately eight times the current value.

d) Although not investigated in the same way as the three other coolant system parameters discussed above, the overall engine temperature changed very significantly with the use of nanofluid coolants. Using base case parameters, the engine temperature dropped from 206 ^{0}C for the base case to 165 ^{0}C for a 2% nanofluid and to 141 ^{0}C for a 4 % nanofluid. These results were due to the increased heat transfer coefficient of the nanofluids in the engine cooling channels. In practice, engine manufactures would probably not use the increased heat transfer coefficient to reduce engine temperature in this way for pollution/emissions reasons. However, the increased heat transfer coefficients of nanofluid coolants give manufacturers great flexibility in the design of engine cooling passages and much more potential for optimizing such difficult factors such as uniform engine block temperature and valve bridge cooling.

Chapter 3

Nanofluids for industrial and nuclear applications

The long term objectives of this project include the experimental determination of the heat transfer enhancement for new water based nanofluids; developing methodologies to prepare stable nanofluids with high heat transfer enhancement; and bulk production of such fluids for industrial and nuclear applications.

This part of the thesis consists of two parts: an experimental component and a modeling and simulation part. Experiments were carried out with water to determine the heat transfer coefficient followed by a thorough numerical modeling analysis using turbulence model with the help of the computational fluid dynamics code FLUENT®. The results obtained from the experiments conducted at the nanofluid heat transfer test facility, which consisted of study of flows with water as the working fluid within the system, are used to benchmark the simulations results. The aim of the work was to benchmark the results for water as the base fluid which would help analyze test results, in the future, with any water based nanofluid for enhancement study characteristics. The numerical analysis is extended to simulate the flows of nanofluids through pipes and results have been presented in comparison to the base fluids. This work will provide the foundation for future work in which both experiments and simulations will be carried out with nanofluids.

The nanofluid-heat-transfer test facility, at Argonne National Laboratory, is designed to experimentally investigate both single- and two-phase heat transfer in small diameter channels with low mass fluxes for nanofluids such as nano-particle in ethylene-glycol and solutions. The facility is described in the next section.

3.1 Experimental setup

The test facility is a closed-loop system which consists of a metering pump with variable speed drive, a preheater, horizontal test section and a counter-flow heat exchanger. The preheater is used to raise the inlet temperature of the fluid to any desired value, before the fluid enters the test section. The system is heated by electrical resistance heating using controllable DC power supplies in both the preheater and the horizontal test section. Fig. 36 shows a schematic diagram of the test facility.

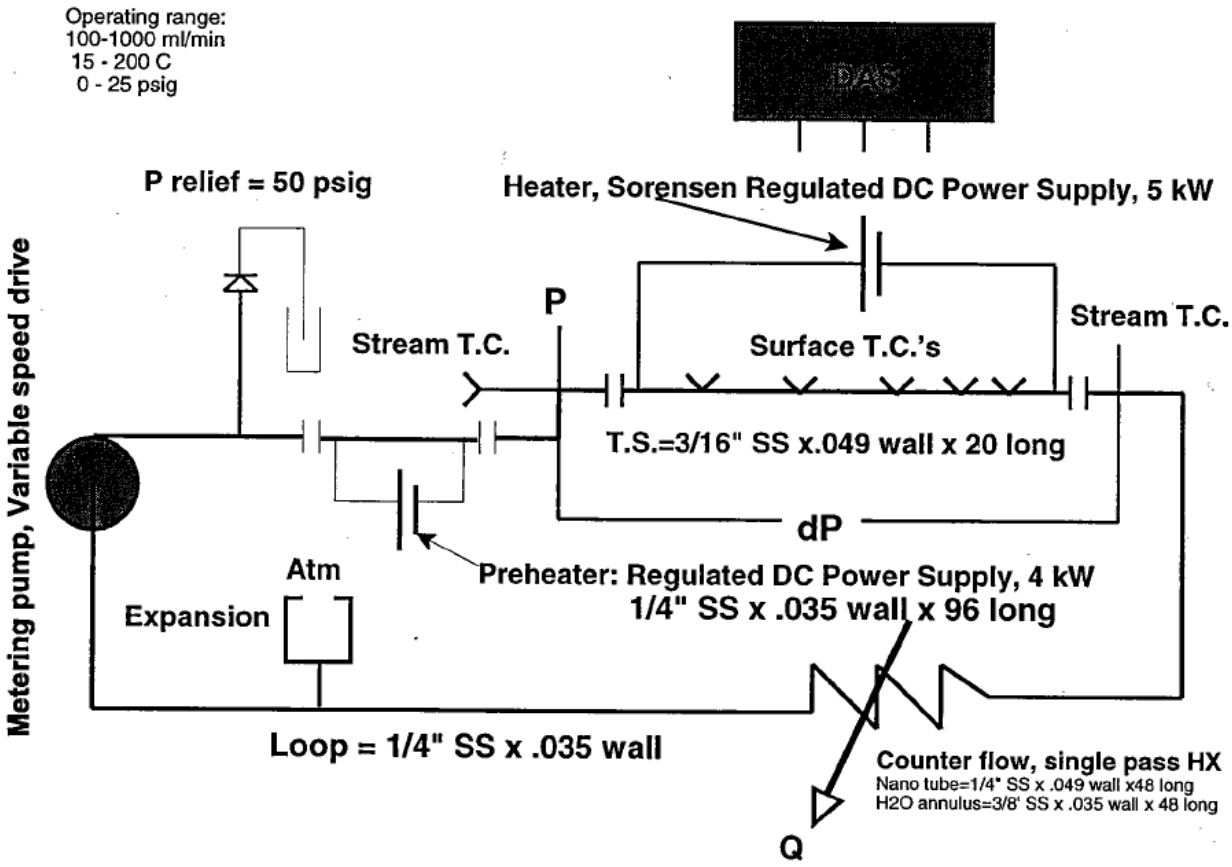

Figure 36. Nanofluid heat transfer test facility setup (source: ANL)

Thermocouples are placed along the test section to measure the wall temperatures at various points as shown in Figure 37.

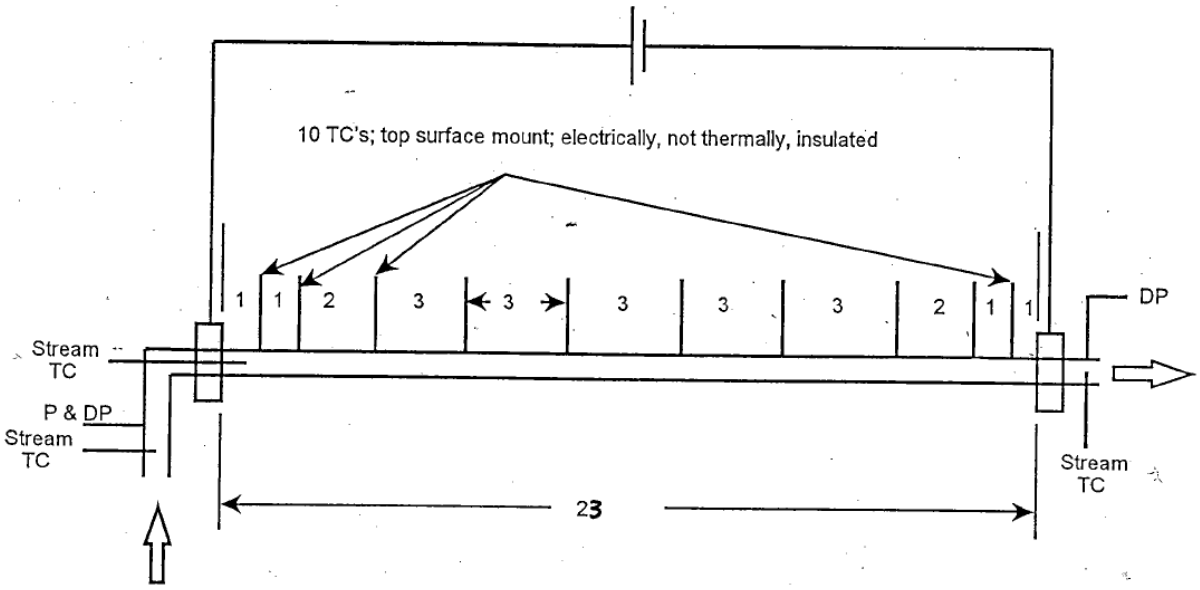

Figure 37. Temperature measurement along the test section (courtesy: ANL)

The wall temperatures measured by the thermocouples are used in the calculation of the heat transfer coefficients along the test section. Pressure and temperature at the inlet and outlet of the test section are also measured and used in this calculation. One thermocouple is inserted into the inlet of the test section to measure the fluid temperature at the inlet of the test section. Based on this fluid temperature and the uniform heating of the test section, the mean fluid temperature can be calculated throughout the test section. The pressure transducers and thermocouples were calibrated against known scales (NIST (National Institute of Standards) traceable) with an estimated uncertainty of ± 3% and ± 0.2 ˚C, respectively. For safety during the tests, both the preheater and the test section are provided with high temperature limit interlocks to prevent from overheating. If the temperature exceeds a certain specified limit, the heaters trip off preventing any potential damage to the test loop components. After leaving the heating section, the fluid is cooled using the counter flow heat exchanger. The heat exchanger is of annular form. The test

fluid runs through the inner tube and the tap water (cooling fluid) runs in the opposite direction through the outer annulus of the heat exchanger. Based on the temperatures achieved in the test section, cooling can be provided by adjusting the mass flow rate of tap water. The test fluid at the exit of the cooling section is re-circulated back to the preheater through the pump. A picture of the experimental setup is shown in Figure 38.

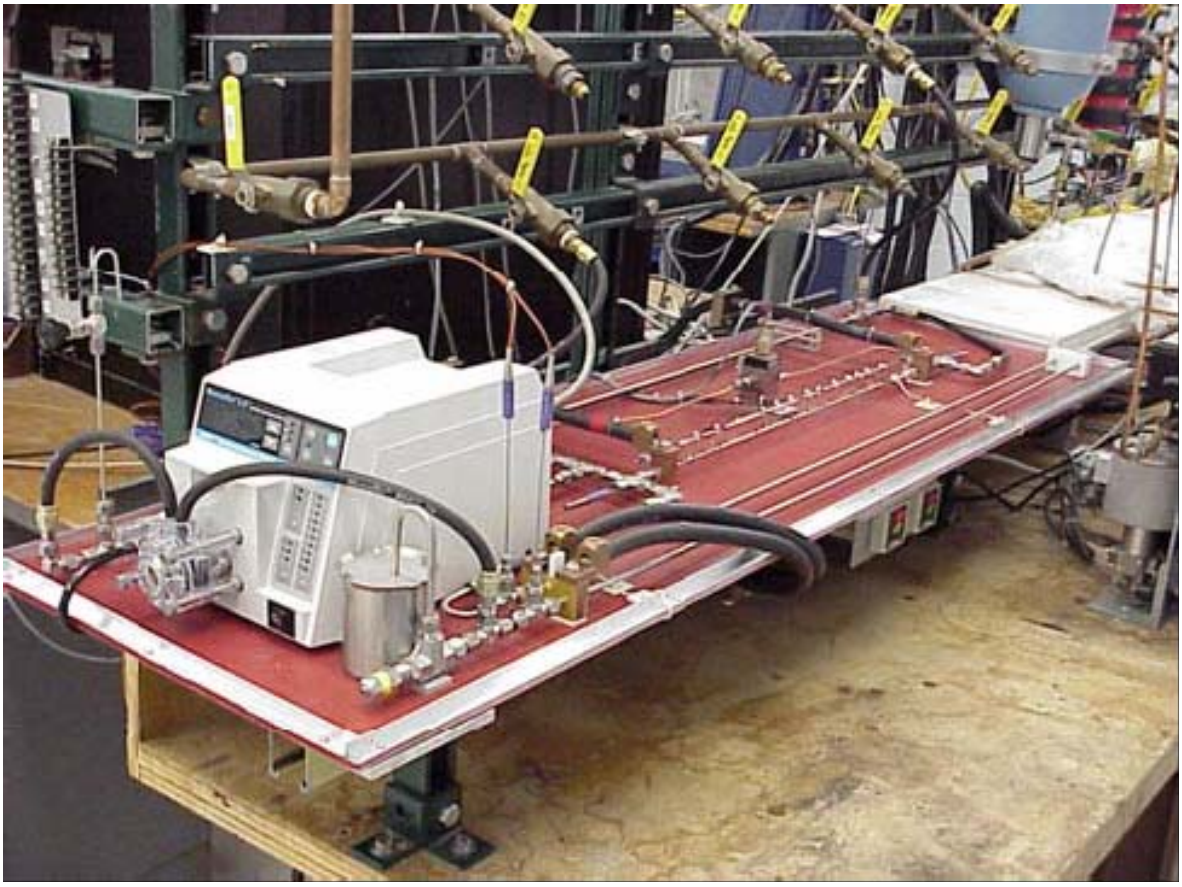

Figure 38. Experimental setup at ANL (source : ANL)

The outputs from all the sensors are recorded using a data acquisition system consisting of a Hewlett-Packard multiplexer and a computer. The computer has a data acquisition program which has inbuilt calibration equations for interpreting the various data collected

from the experiments. Various parameters like mass flux, input power, inlet pressure, pressure drop, temperatures at various points in the loop etc. are also recorded by the data acquisition system. Experiments were conducted using water. Experimental procedure is given in Appendix A.

3.2 Experimental results

Experiments were performed for different Reynolds numbers in the turbulent flow regime over a range of temperature to characterize the base flow with water as the working fluid. This base flow can subsequently be used to compare the heat transfer characteristics of nanofluid flow and its effects on heat transfer.

The experimental results for water are shown in Table 9. This table illustrates the important data for various tests. All the data represent the mean values for various parameters over the length of the test section. In the experiments, the flow rate is measured using a calibrated flow meter. Thermocouples have been set to measure the fluid mean temperature at inlet and the outer wall temperatures at various points in the test section as shown in Fig. 37. The total power input to the test section is calculated from the voltage and current applied to the test section. From these experimental data, various other parameters are calculated. The average velocity is calculated by dividing the flow rate with the cross-sectional area. The wall heat flux is calculated based on the dimensions of the test section (length and the inner radius) and the total heat input into the test section. The fluid mean temperature at the inlet of the test section is noted from

the thermocouple reading. Based on a simple energy balance, the fluid mean temperature at any cross-section is calculated using the average wall heat flux and the mass flow rate of coolant. The experimental heat transfer coefficient is calculated as the ratio between the average wall heat flux and the fluid mean temperature difference.

Table 9. Experimental results with water as the working fluid

Sr. No.	Difference between wall and fluid mean temperature (^{0}C)	Wall heat flux (W/m^2)	Experimental heat transfer Coefficient (W/m^2-K)	Average Velocity (m/s)	Reynolds number	Prandtl number	Nusselt number
1	9.46	1.21E+05	1.32E+04	1.83	5.76E+03	4.86	47.98
2	15.61	2.18E+05	1.44E+04	1.90	7.13E+03	4.06	51.30
3	17.50	1.91E+05	1.12E+04	1.51	5.80E+03	3.98	40.09
4	16.33	2.45E+05	1.53E+04	2.11	8.05E+03	3.98	54.70
5	15.55	2.74E+05	1.79E+04	2.52	9.68E+03	3.94	63.77
6	14.25	2.96E+05	2.11E+04	2.92	1.12E+04	3.93	75.21
7	13.48	3.20E+05	2.40E+04	3.32	1.28E+04	3.91	85.68
8	12.96	3.50E+05	2.73E+04	3.73	1.45E+04	3.85	97.19

3.3 Numerical modeling of experimental test section

The objective of this study was to benchmark the results obtained using a CFD code like FLUENT® with the experimental results for the water tests. These numerical results, once benchmarked, provide the base case for comparison against other simulation results

obtained for nanofluids simulated by changing the properties of the base fluid to a nanofluid for similar flow conditions.

A cylindrical test section of radius 1.13665 mm and length of 558.8 mm is modeled. These dimensions correspond to that of the actual test section. The grid for this problem was created using GAMBIT® with a quad type mesh. A graded grid size is used both in the axial and radial directions. In the radial direction, as shown in Fig. 39, a graded grid consisting of 20 nodes is used with the first cell height of 0.2% of the radius of the test-section. In the axial direction a total of 1000 nodes are used with a growth ratio of 1.003.

Figure 39. Graded grid in the radial direction as created in GAMBIT(R)

3.4 Problem definition and solution methodology in FLUENT® modeling

The flow through the test section was modeled in FLUENT® as a fully developed, steady-state, 2-D, axisymmetric pipe flow. The k-ω model [Wilcox, 1988] is used to for turbulence. A constant heat flux is imposed at the wall of the cylindrical section. Numerical values of the heat flux used correspond to the actual heat input into the test section in the experimental tests. The average velocity of the incoming flow (calculated from the overall volume flow rate and the cross-sectional area of test-section) and the fluid mean temperature are specified at the inlet of the test section. The exit of the test section is kept at the outflow conditions which represent the fully developed flow regime

A segregated solver is used in FLUENT® to solve the flow equations. First, we solve only the flow equations with the energy equation turned 'off' till the flow field variables have reached convergence. The convergence criterion is kept at the order of 10^{-6} for all the variables viz. continuity, x-velocity, y-velocity, k and omega. Once the flow equations have converged, the energy equation is turned on and the iterations are continued with all the equations with the same convergence criterion as above. For all these simulations the properties of the working fluid have been assumed to be constant and evaluated at the fluid mean temperature in the middle of the test section.

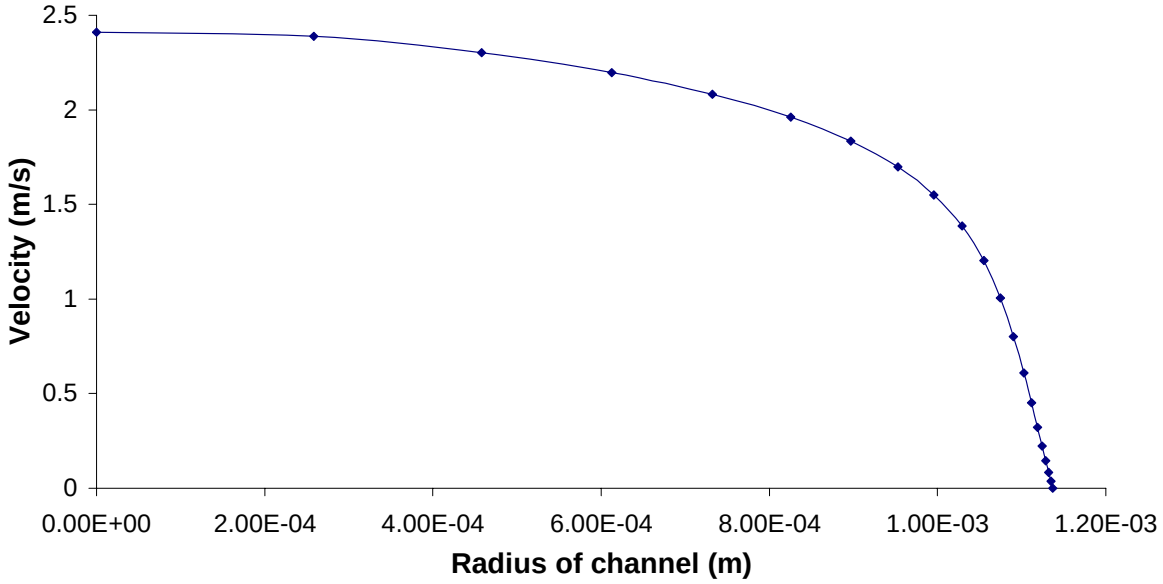

Figure 40. Fully developed velocity profile in the radial direction within the test section

In Fig. 40, the fully developed velocity profile for case 1 of Table 6 has been plotted as a function of the radial position. The distribution of points also illustrates the non-uniform grid in the radial direction. The non-uniform grid allows a smaller number of grid points to capture the steep variation in velocity near the wall. The numerical results for both fluid flow and heat transfer showed no significant change with further refinement in grid sizes (both along axial and radial directions). The grid size has been mentioned previously in section 3.3 of this chapter.

In Fig. 41, the temperature profile for water (case 1) at a section 0.3 m inside the test section (starting from the inlet) is shown. The non-uniform grid in the radial direction is able to capture the steep gradient in temperature near the wall. Also, it should be noted

that the temperature within the bulk of the liquid is almost a constant as compared to the region near the wall.

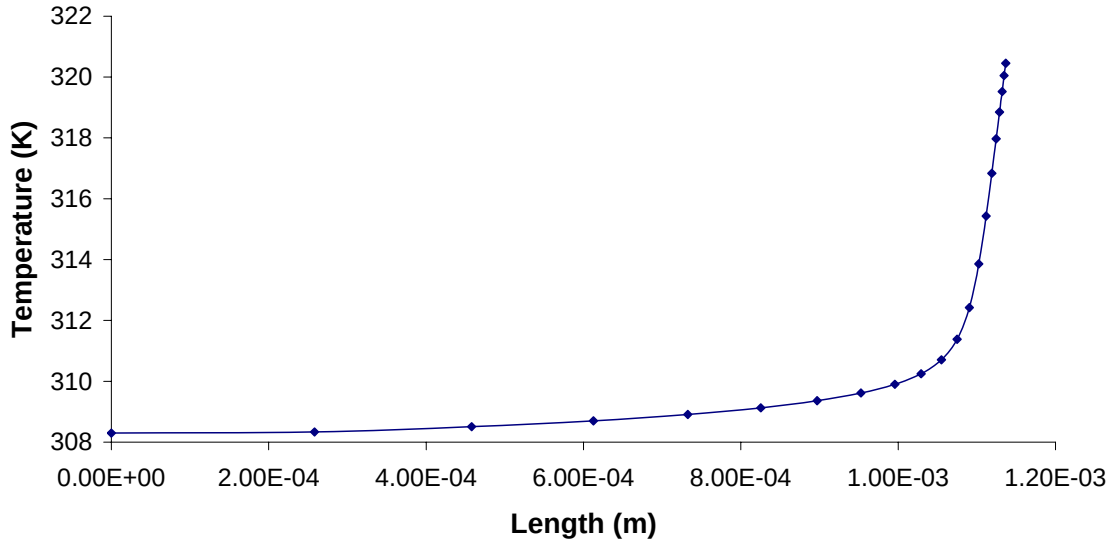

Figure 41. Fully developed temperature profile for water at a cross-section of 0.3 m from the entrance

In Figure 42, the increase in temperature along the length of the test section is illustrated. The plot specifically shows the centerline (axis) and the wall temperatures for case 1 along the test section. From the results of the k- ω model we can infer that after changing over the (small) developing flow region, the temperature difference between the wall and the centerline becomes almost a constant which implies that the flow is fully developed and the heat coming in from the wall is increasing the local fluid temperatures linearly.

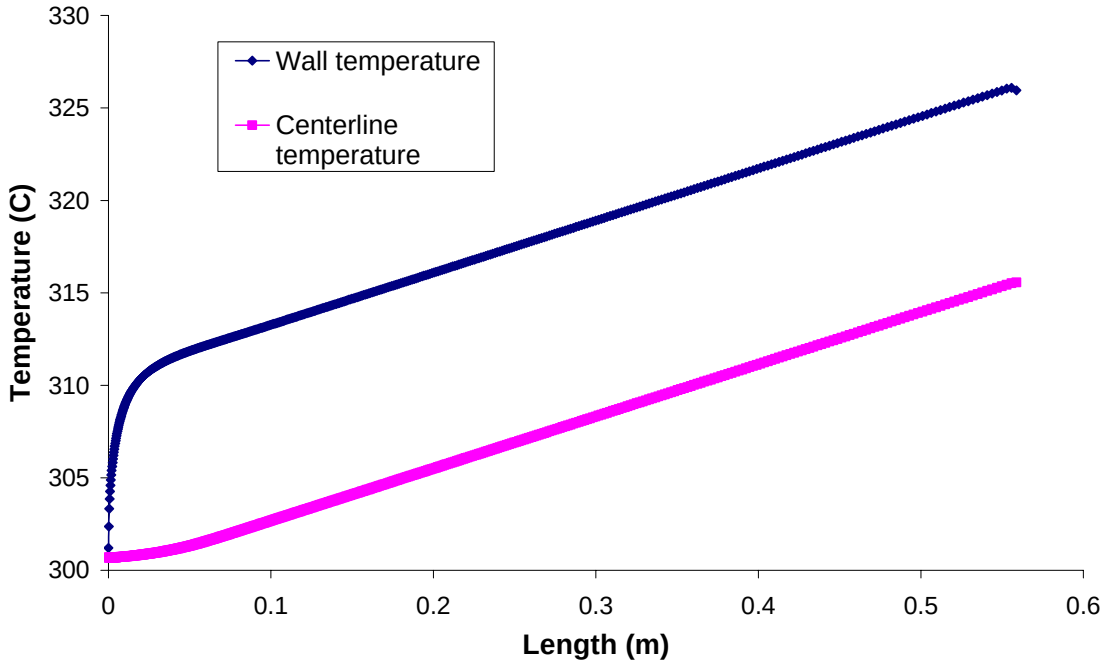

Figure 42. Temperature increase along the length of the test section for case 1 in Table 9

3.5 Benchmarking of numerical results with the experimental tests

To validate the numerical analysis performed for the study of heat transfer enhancements of nanofluids, the numerical results are compared with the results of the experimental tests reported in chapter 2. In Table 10, a comparison between the results of the experimental analysis and numerical modeling is shown. It is observed that the percent deviation of the numerical results from the experimental data is moderate with a maximum deviation being about 11%. The deviation may be attributed to the fact that the fluid properties are assumed not to vary with temperature, while there is a significant change in temperature between the inlet and exit of the flow domain. In the modeling, the viscosity of the fluid was calculated for each case, based on an average fluid temperature

calculated over the length of the test section based on overall energy balance and the inlet fluid temperature. The viscosity plays a significant role in determining the heat transfer and hence the value of the Nusselt number.

Table 10. Comparison of average Nusselt number from experiments and numerical modeling data

CASE	Dynamic Viscosity (numerical)	Average Nusselt number (numerical)	Average Nusselt number (experimental)	Percent difference in Nusselt numbers
1	0.000724	48.13	47.98	0.293449
2	0.000615	53.12	51.30	3.558281
3	0.000603	44.76	40.09	11.6592
4	0.000603	58.05	54.70	6.109162
5	0.000599	67.05	63.77	5.156247
6	0.000597	75.41	75.21	0.257047
7	0.000594	83.67	85.68	-2.35082
8	0.000587	92.34	97.19	-4.99368

In Table 10, the Nusselt number is calculated numerically by extracting the temperature of the node near the wall based on flow conditions from FLUENT®. A Neumann kind of boundary condition is maintained at the wall for the temperature distribution. The mass flux based averaged temperature is calculated at the cross-section from the code. The ratio between the wall heat flux and the difference between the near wall temperature and the mean fluid temperature gives us the heat transfer coefficient at the section. From the heat transfer coefficient the Nusselt number is calculated using the dimensions of the test section and the thermal conductivity of the fluid.

Based on the confidence that the numerical simulations predict the experimental results for the water-only case, the same model is applied to simulate the nanofluids to compare the potential heat transfer enhancements for various cases under consideration.

3.6 Numerical modeling of heat transfer in nanofluid and comparison with the pure water case

In this section, the comparison between water and the nanofluid (with 40% enhancement in thermal conductivity) is presented for the various cases. For the properties of the hypothetical nanofluid, only the thermal conductivity is enhanced by 40% i.e. k = 0.84 W/m^2-K is used as compared to k = 0.6 W/m^2-K for water. In Fig. 43, a comparison is made between the heat transfer characteristics of the nanofluid as compared to pure water for similar flow and heat conditions. It is observed that there is a decrease (about 10% approximately) in the Nusselt number for a given Reynolds number.

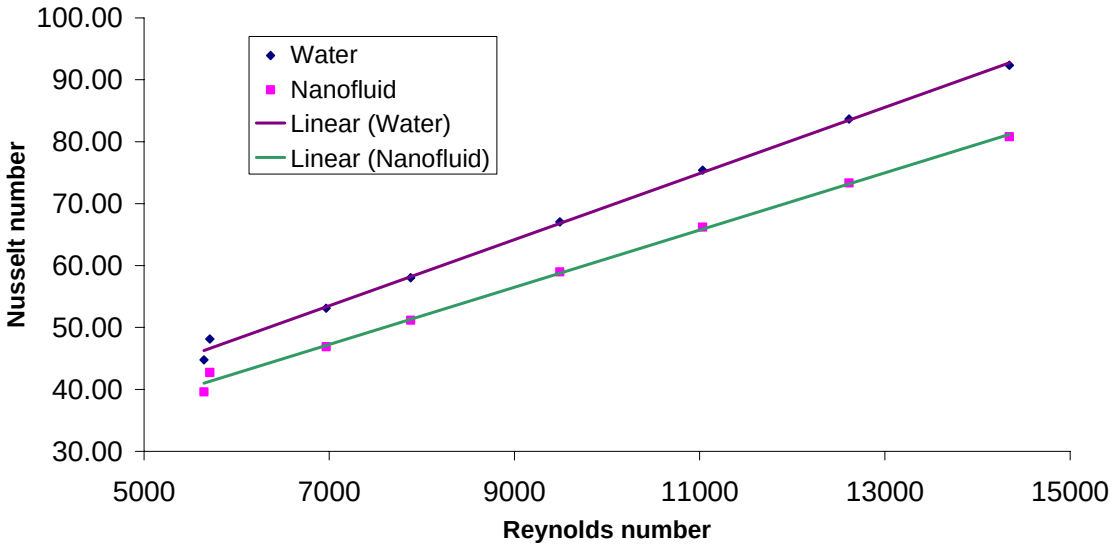

Figure 43. Comparison of heat tranasfer characteristics between water and nanofluid

In Fig. 44, the heat transfer coefficient for water and the nanofluid are compared. We observe that though there is a decrease in the Nusselt number for a given Reynolds number for the nanofluid, there is an increase in the overall heat transfer coefficient (about 30% on average) which implies improved heat transfer within the system.

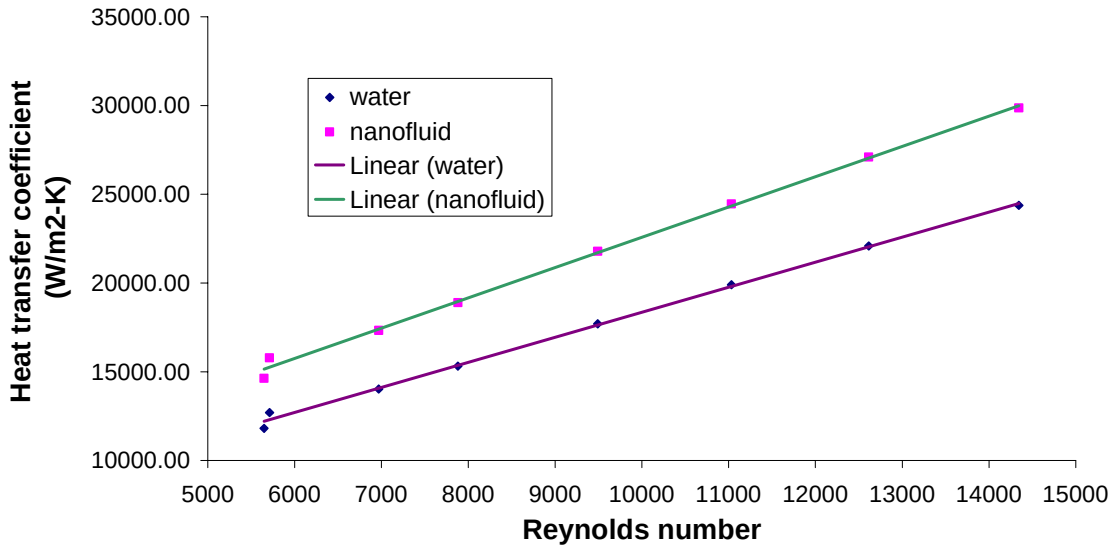

Figure 44. Comparison of heat transfer coefficient between water and nanofluid

3.7 Comparison of various nanofluids for a given flow condition

In this section, heat transfer characteristics are analyzed numerically for a given flow condition (case 1) by varying the conductivity over the range from 0-40% of the base fluid (water, in this study).

In Fig. 45, the variation of Nusselt number is shown for given flow conditions for nanofluids with different thermal conductivity properties. In these simulations, the other

fluid properties have been assumed to be constant to compare the data with the base fluid (water in our case).

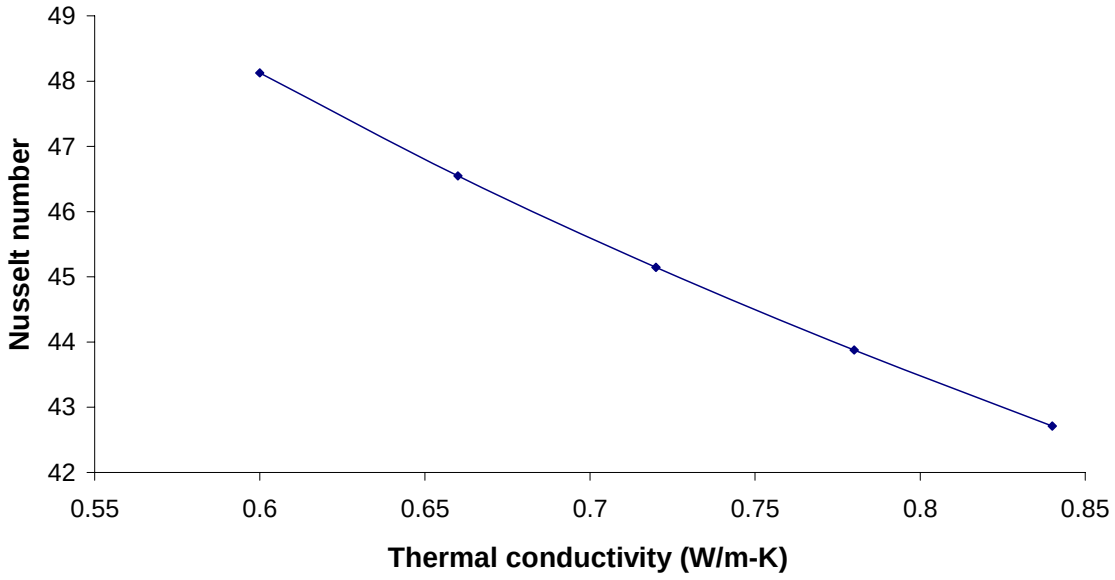

Figure 45. Nusselt number as a function of thermal conductivity for flow conditions corresponding to Case 1 in Table 9

Variation in the heat transfer coefficient due to the thermal conductivity changes are shown in Fig. 46. Note that there is a steady increase in heat transfer coefficient as the thermal conductivity increases. This supports our belief that nanofluids would perform as better heat transfer coolants compared to their respective base fluids.

The results of Figs. 45 and 46 show a decrease in Nusselt number and an increase in heat transfer coefficient as the particle concentration increases in the nanofluid. Experimental results [Yu et al. 2007] show that both increase. The difference is due to the way in which the nanofluid was modeled in this analysis. In the analysis, only the effect of increased thermal conductivity of the nanofluid was considered as particle concentration increased

in the nanofluids. The experimental results point to additional heat transfer enhancement due to particle-fluid and/or particle-particle interactions. However, the results of the analysis predict the correct trend for the heat transfer coefficient if not the experimentally observed magnitude. This heat transfer coefficient trend governs the heat transfer enhancement of nanofluids over their base fluids, and it is clear that the thermal conductivity enhancement alone is sufficient to produce the observed trend. For this reason, many experimenters only measure the thermal conductivity and not the heat transfer coefficient of nanofluids. The former is much easier to measure and is a good indicator of the heat transfer enhancement of the nanofluid.

In the last plot (Fig. 47), the temperature profiles are shown at a given cross-section (0.3 m from the inlet) for various nanofluids and the base-fluid (water). Looking at the plot carefully, it can be seen that there is a small difference in temperature near the wall which corresponds to the fact that the fluids with lower thermal conductivity have steeper thermal gradient near the wall.

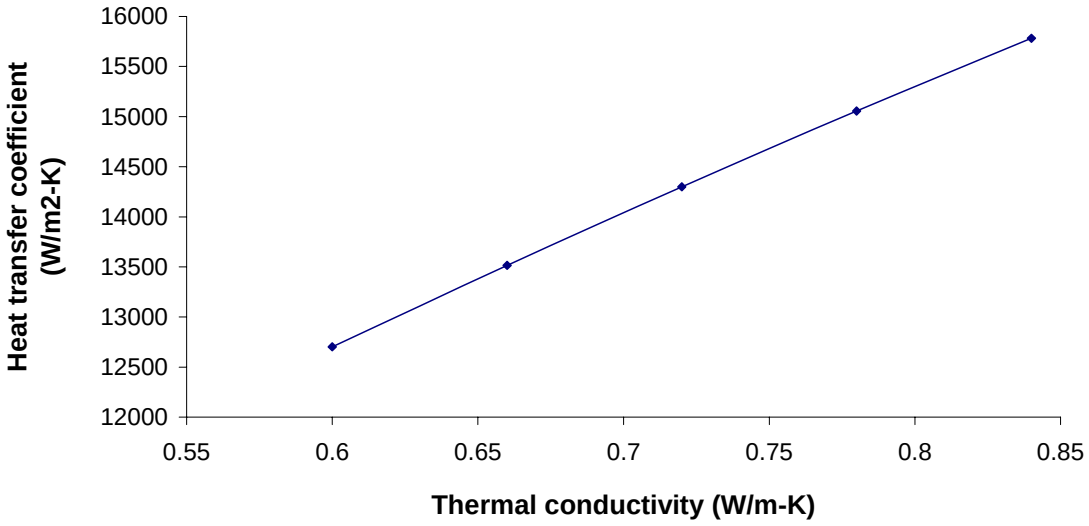

Figure 46. Heat transfer coefficient as a function of thermal conductivity

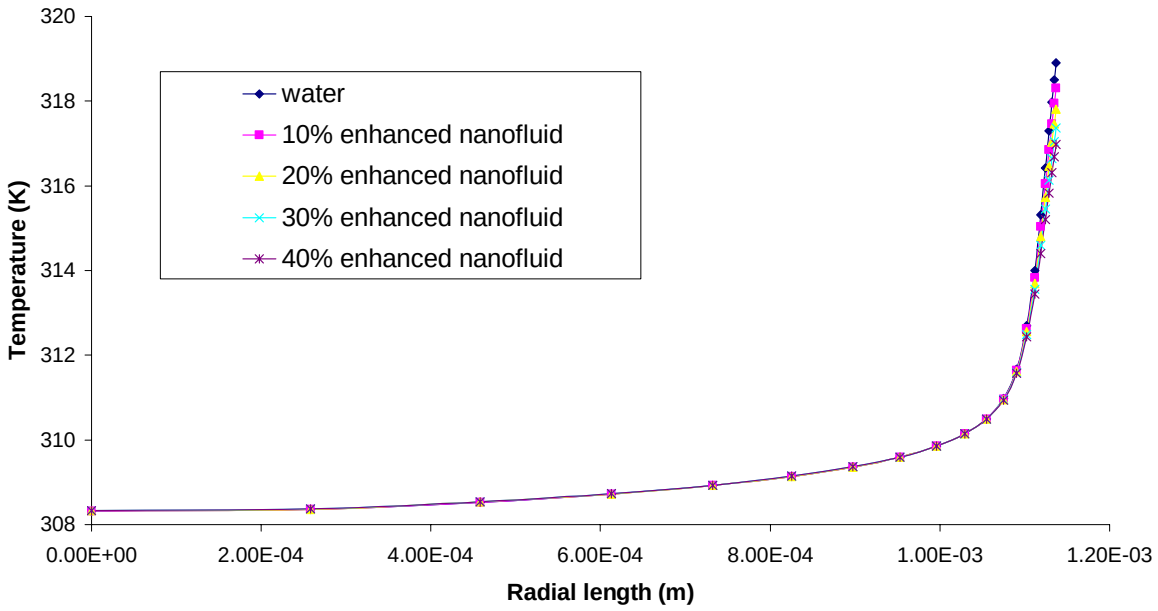

Figure 47. Comparison of cross-sectional temperature profiles for given flow conditions

3.8 Discussion

The nanofluid test facility built at Argonne National Laboratory is well designed for understanding the heat transfer characteristics of nanofluids. Based on the benchmarking of simulation results with the experimental observations, it can be concluded that the predictions using the k-ω model for turbulence match well with the experimental data taken from the nanofluid test facility at Argonne National Laboratory.

Moreover, from the various numerical modeling results obtained using the CFD code FLUENT® we can conclude that the nanofluids improve the heat transfer coefficient (about 30% increase) even though the Nusselt number decreases (about 10% drop). This is due to the fact that Nusselt number depends upon both, the thermal conductivity and the heat transfer coefficient, and though thermal conductivity and heat transfer coefficient are both higher for the nanofluid by about 40% and 30 % respectively (than the base fluid), the larger increase in the thermal conductivity than the increase in heat transfer coefficient leads to a drop (of about 10%) in the Nusselt number for the nanofluid. The relationship in thermal conductivity, heat transfer coefficient and Nusselt number for the base and nanofluid cases can be illustrated by the definition of the Nusselt number

$$Nu = \text{ Nusselt Number} = \frac{hD}{k}$$

$$\frac{Nu_2}{Nu_1} = \frac{\left(h_2 \big/ h_1 \right)}{\left(k_2 \big/ k_1 \right)} \Rightarrow \frac{h_2}{h_1} = \left(\frac{Nu_2}{Nu_1} \right) \left(\frac{k_2}{k_1} \right)$$

Here, subscript 1 represents the base fluid and subscript 2 represents the nanofluid.

Hence, a 40% increase in k and a 10% decrease in Nusselt number imply an approximate increase of about 30% in the heat transfer coefficient.

These numerical and experimental results quantify the possible increase in both the conductive and convective heat transfer modes and hence confirm the potential of nanofluids as effective coolants.

Chapter 4

Conclusions

Fluid flow and heat transfer are integral part of nuclear thermal-hydraulic processes. Attempts made to enhance the heat transfer process always leads to an improvement in the overall thermal efficiency and hence the performance of the overall system. Nanofluids are modern technology fluids engineered to cater to the ever increasing demand to remove higher heat fluxes at lower cost. These applications range from small scale applications like cooling in notebook computers to the large scale nuclear reactor. Heat transfer and fluid flow principles have applications in a wide range of industries viz. transportation, electronics, medical, manufacturing as well as nuclear power engineering.

In this thesis, an attempt has been made to quantify the potential heat transfer enhancement of nanofluids as replacement for existing coolants in various scenarios. As an example of an engineering application, the modern truck coolant circuit was chosen. The potential enhancements of the coolant circuit include;

1. Increase in engine heat rejection (up to 5%);
2. Reduction in radiator air-side area (up to 5%); and
3. Coolant pump power reduction (by about a factor of 8).

The results obtained using the commercial code FLOWMASTER® help in quantifying the potential of nanofluids.

During the course of the project, experiments were performed at the nanofluid test facility at Argonne National Laboratory with water as the base fluid for testing and verification purposes. These results have been compared to simulations carried out using FLUENT® to benchmark the numerical simulations. After benchmarking the simulations, a nanofluid was simulated to analyze the potential enhancements due to the nanofluid with respect to base fluids. The results obtained using the numerical simulations show that though a decrease in Nusselt number (about 10%) is observed for the nanofluid with similar flow conditions as the base fluid, the heat transfer coefficient is actually enhanced by about 30% when a nanofluid with thermal conductivity that is higher by about 40% over the base fluid is used.

Experimental results [Yu et al. 2007] have shown enhancement in both the Nusselt number and the thermal conductivity for nanofluids. Both scenarios support the fact that for a given flow condition, the nanofluid would be a better coolant compared to the base fluid as both the thermal conductivity and the overall heat transfer coefficient show an enhancement.

Based on the results from the numerical modeling exercise a conclusion can be made that nanofluids show significant potential for heat transfer enhancement and this thesis attempts to quantify such claims made by researchers. Specific examples have been considered pertaining to the automotive cooling system. These results can be generalized to any other system like the nuclear steam supply system (NSSS).

4.1 Scope for future work

Currently, the potential of nanofluids has been studied numerically for the automotive coolant system as an example. A logical step would be to apply similar modeling principles to a specific nuclear steam supply system and analyze the potential enhancements. Also, the current study was confined to single-phase flow of the coolant. It would be interesting to look at models which incorporate the two-phase flow effects as the critical heat flux (CHF) has been shown to be enhanced experimentally for nanofluids which would be an added point of advantage for the nuclear research and development community.

In the k-ω model for turbulent flows, incorporated in FLUENT® there exists a limitation of using constant properties for the working fluid. To have a better understanding of the performance of the nanofluid, it may be a good idea to develop an in-house code of the k-ω model incorporating the temperature dependent properties of the working fluid. Also, experimental results have shown enhancement in both the Nusselt number and thermal conductivity of the nanofluid whereas the numerical modeling using k-ω model shows a decreasing trend for the Nusselt number. This model can be modified to include particle-particle or particle-fluid interactions to look for improvement in predictions for comparison with experimental results for modeling nanofluids.

References

Benveniste, Y. 1987. Effective Thermal Conductivity of Composites with a Thermal Contact Resistance between the Constituents: Nondilute Case, *Journal of Applied Physics,* vol. 61, pp. 2840-2843.

Benveniste, Y., and Miloh, T. 1991. On the Effective Thermal Conductivity of Coated Short-Fiber Composites. *Journal of Applied Physics,* vol. 69, pp. 1337-1344.

Böttcher, C. J. F. 1945. The Dielectric Constant of Crystalline Powders. *Recueil des Travaux Chimiques des Pays-Bas,* vol. 64, pp. 47-51.

Bruggeman, D. A. G. 1935. Berechnung verschiedener physikalisher Konstanten von heterogenen Substanzen: I. Dielektrizitätskonstanten und Leitfähigkeiten der Mischkörper aus isotropen Substanzen. *Annalen der Physik,* vol. 24, pp. 636-664.

Buongiorno, J. and Hu, L.-W. 2005. Nanofluid Coolants for Advanced Nuclear Power Plants. Paper 5705, *Proceedings of ICAPP '05*, Seoul, May 15-19

Buongiorno, J. and Truong, B. 2005. Potential of Water-based Nanofluids for Use as Coolants in PWRs. Paper # 525, *Proceedings of the 11th International Topical Meeting on Nuclear Reactor Thermal-Hydraulics (NURETH-11)*, Avignon, France, October 2-6.

Buongiorno J., Hu, L.-W., Kim, S. J., Hannink, R., Truong, B. and Forrest, E. 2006. Use of nanofluids for enhanced economics and safety of nuclear reactors. *COE-INES International Symposium*, INES-2 Yokohama, November 26-30.

Choi, S. U. S. 1995. Enhancing Thermal Conductivity of Fluids with Nanoparticles. *Developments and Applications of Non-newtonian Flows,* eds. D. A. Singer and H. P. Wang, vol. FED 231, pp. 99-105, American Society of Mechanical Engineers, New York.

Choi, S. U.-S., Lee, S., Li, S., and Eastman, J. A., 1999. Measuring Thermal Conductivity of Fluids Containing Oxide Nanoparticles. *Transactions of the ASME, Journal of Heat Transfer,* vol. 121, pp. 280-289.

Choi, S. U. S., Zhang, Z. G., Yu, W., Lockwood, F. E., and Grulke, E. A. 2001. Anomalously Thermal Conductivity Enhancement in Nanotube Suspensions. *Applied Physics Letters,* vol. 79, pp. 2252-2254.

Choi, S. U. S., Zhang, Z. G., and Keblinski, P., 2004. Nanofluids. *Encyclopedia of Nanoscience and Nanotechnology,* ed. H. S. Nalwa, vol. 6, pp. 757-737, American Scientific Publishers, Los Angles, California, USA.

Das, S. K. 2006. Nanofluids – The Cooling Medium of the Future. *Heat Transfer Engineering,* vol. 27, no. 10, pp. 1-2.

Das, S. K., Choi, S. U. S., and Patel, H. E. 2006. Heat Transfer in Nanofluids – A Review. *Heat Transfer Engineering,* vol. 27, no. 10, pp. 3-19.

Das, S. K., Putra, N., Thiesen, P., and Roetzel, W. 2003. Temperature Dependence of Thermal Conductivity Enhancement for Nanofluids. *Transactions of the ASME, Journal of Heat Transfer,* vol. 125, pp. 567-574.

Davis, R. H. 1986. The Effective Thermal Conductivity of a Composite Material with Spherical Inclusions. *International Journal of Thermophysics,* vol. 7, pp. 609-620.

Dittus, F. W., and Boelter, L. M. K. 1930. Heat Transfer in Automobile Radiators of the Tubular Type, *University of California Publications in Engineering,* vol. 2, pp. 443-461.

Eastman, J. A., Phillpot, S. R., Choi, S. U. S., and Keblinski, P. 2004. Thermal Transport in Nanofluids. *Annual Revies in Material Research,* vol. 34, pp. 219-246.

Einstein, A. 1906. Eine neue Bestimmung der Moleküldimensionen. *Annalen der Physik,* vol. 19, pp. 289-306.

Flowmaster, Inc., www.Flowmaster.com

Fricke, H. 1924. A Mathematical Treatment of the Electric Conductivity and Capacity of Disperse Systems: I. The Electric Conductivity of a Suspension of Homogeneous Spheroids. *Physical Review,* vol. 24, pp. 575-587.

Fricke, H., 1935. The Maxwell-Wagner Dispersion in a Suspension of Ellipsoids. *Journal of Physical Chemistry,* vol. 57, pp. 934-937.

Granqvist, C. G., and Hunderi, O. 1977. Optical Properties of Ultrafine Gold Particles. *Physical Review B,* vol. 16, pp. 3513-3534.

Granqvist, C. G., and Hunderi, O. 1978. Conductivity of Inhomogeneous Materials: Effective-Medium Theory with Dipole-Dipole Interaction. *Physical Review B,* vol. 18, pp. 1554-1561.

Hamilton, R. L., and Crosser, O. K. 1962. Thermal Conductivity of Heterogeneous Two-Component Systems. *Industrial & Engineering Chemistry Fundamentals,* vol. 1, pp. 187-191.

Hasselman, D. P. H., and Johnson, L. F. 1987. Effective Thermal Conductivity of Composites with Interfacial Thermal Barrier Resistance, *Journal of Composite Materials,* vol. 21, pp. 508-515.

Heris, S. Z., Etemad, S. Gh., and Esfahany, M. N. 2006. Experimental Investigation of Oxide Nanofluids Laminar Flow Convective Heat Transfer. *International Communications in Heat and Mass Transfer,* vol. 33, pp. 529-535.

Jang, S. P., and Choi, S. U. S. 2004. Role of Brownian Motion in the Enhanced Thermal Conductivity of Nanofluids. *Applied Physics Letters,* vol. 84, pp. 4316-4318.

Jeffrey, D. J. 1973. Conduction through a Random Suspension of Spheres. *The Proceedings of Royal Society of London A,* vol. 335, pp. 355-367

Keblinski, P., Eastman, J. A., and Cahill, D. G. 2005. Nanofluids for Thermal Transport. *Materials Today,* pp. 36-44.

Kerner, E. H. 1956. The Electrical Conductivity of Composite Media. *The Proceedings of the Physical Society B,* vol. 69, pp. 802-807.

Koo, J., and Kleinstreuer, C. 2004. A New Thermal Conductivity Model for Nanofluids. *Journal of Nanoparticle Research,* vol. 6, pp. 577-588.

Lamb, W., Wood, D. M., and Ashcroft, N. W. 1978. Optical Properties of Small Particle Composites: Theories and Applications, in *Electrical Transport and Optical Properties of Inhomogeneous Media,* ed. by J. C. Garland and D. B. Tanner, pp. 240-255, American Institute of Physics, New York.

Landauer, R. 1952. The Electrical Resistance of Binary Metallic Mixtures. *Journal of Applied Physics,* vol. 23, pp. 779-784.

Lee, S., Choi, S. U.-S., Li, S., and Eastman, J. A. 1999. Measuring Thermal Conductivity of Fluids Containing Oxide Nanoparticles. *Transactions of the ASME, Journal of Heat Transfer,* vol. 121, pp. 280-289.

Lu, S.-Y., and Song, J.-L. 1996. Effective Conductivity of Composites with Spherical Inclusions: Effective of Coating and Detachment, *Journal of Applied Physics,* vol. 79, pp. 609-618.

Maxwell, J. C. 1873. *Treatise on Electricity and Magnetism.* Clarendon Press, Oxford, UK.

Pauly, von H., and Schwan, H. P. 1959. Über die Impedanz einer Suspension von kugelförmigen Teilchen mit einer Schale. *Zeitschrift für Naturfarschung,* vol. 146, pp. 125-131.

Pak, B. C., and Cho, Y. I. 1998. Hydrodynamic and Heat Transfer Study of Dispersed Fluids with Submicron Metallic Oxide Particles, *Experimental Heat Transfer,* vol. 11, pp. 151-170.

Polder, D., and van Santen, J. H. 1946. The Effective Permeability of Mixtures of Solids. *Physica,* vol. 12, pp. 257-271.

Prasher, R., Bhattacharya, P., and Phelan, P. E. 2005. Thermal Conductivity of Nanoscale Colloidal Solutions (Nanofluids), *Physical Review Letters,* vol. 94, paper number 025901, 4 pp.

Prasher, R., Bhattacharya, P., and Phelan, P. E. 2006a. Brownian-Motion-Based Convective-Conductive Model for the Thermal Conductivity of Nanofluids, *Transaction of the ASME, Journal of Heat Transfer,* vol. 128, pp. 588-595.

Prasher, R., Phelan, P. E., and Bhattacharya, P. 2006b. Effect of Aggregation Kinetics on the Thermal Conductivity of Nanoscale Colloidal Solutions (Nanofluid), *Nano Letters,* vol. 6, pp. 1529-1534.

Rayleigh, L. 1892. On the Influence of Obstacles Arranged in Rectangular Order upon the Properties of a Medium. *Philosophical Magazine,* vol. 34, pp. 481-502.

Ren, Y., Xie, H., and Cai, A. 2005. Effective Thermal Conductivity of Nanofluids Containing Spherical Nanoparticles. *Journal of Physics D: Applied Physics,* vol. 38, pp. 3958-3961.

Schwan, H. P., Schwarz, G., Maczuk, J., and Pauly, H. 1962. On the Low-Frequency Dielectric Dispersion of Colloidal Particles in Electrolyte Solution, *Journal of Physical Chemistry,* vol. 66, pp. 2626-2635.

Taylor, L. S. 1965. Dielectrics Properties of Mixtures. *IEEE Transactions on Antennas and Propagation,* vol. AP-13, pp. 943-947.

Taylor, L. S. 1966. Dielectrics Loaded with Anisotropic Materials. *IEEE Transactions on Antennas and Propagation,* vol. AP-14, pp. 669-670.

Van de Hulst, H. C. 1957. *Light Scattering by Small Particles.* John Wiley & Sons, New York.

Wang, X., Xu, X., and Choi, S. U. S. 1999. Thermal Conductivity of Nanoparticle-Fluid Mixture. *Journal of Thermophysics and Heat Transfer,* vol. 13, pp. 474-480.

Wang, B.-X., Zhou, L.-P., and Peng, X.-F. 2003. A Fractal Model for Predicting the Effective Thermal Conductivity of Liquid with Suspension of Nanoparticles, *International Journal of Heat and Mass Transfer,* vol. 46, pp. 2665-2672.

Wiener, O. 1912. Die Theorie des Mischkörpers für das Feld der stationären Strömung, 1. Abhandlung: Die Mittelwertsätze für Kraft, Polarisation und Energie. *Der Abhandlungen*

der Mathematisch-Physischen Klasse der Königlich Sächsischen Gesellschaft der Wissenschaften, vol. 32, pp. 507-604.

Wilcox, D.C. 1988. Re-assessment of the scale-determining equation for advanced turbulence models, *AIAA Journal*, vol. 26, pp. 1414-1421.

Xie, H., Wang, J., Xi, T., and Liu, Y. 2002a. Thermal Conductivity of Suspensions Containing Nanosized SiC Particles, *International Journal of Thermophysics,* vol. 23, pp. 571-580.

Xie, H., Wang, J., Xi, T., and Ai, F. 2002b. Thermal Conductivity Enhancement of Suspensions Containing Nanosized Alumina Particles, *Journal of Applied Physics,* vol. 91, pp. 4568-4572.

Xie, H., Wang, J., Xi, T., Liu, Y., and Ai, F. 2002c. Dependence of the Thermal Conductivity of Nanoparticle-Fluid Mixture on the Base Fluid. *Journal of Materials Science Letters,* vol. 21, pp. 1469-1471.

Xie, H., Fujii, M., and Zhang, X. 2005. Effect of Interfacial Nanolayer on the Effective Thermal Conductivity of Nanoparticle-Fluid Mixture. *International Journal of Heat and Mass Transfer,* vol. 48, pp. 2926-2932.

Xuan, Y., and Li, Q. 2003. Investigation on Convective Heat Transfer and Flow Features of Nanofluids. *Transactions of the ASME, Journal of Heat Transfer,* vol. 125, pp. 151-155.

Xue, Q. 2000. Effective-Medium Theory for Two-Phase Random Composite with an Interfacial Shell. *Journal of Material Science and Technology,* vol. 16, pp. 367-369.

Yang, B., and Han, Z. H. 2006. Temperature-Dependent Thermal Conductivity of Nanorod-Based Nanofluids. *Applied Physics Letters,* vol. 89, paper number 083111, 3 pp.

You, S. M., Kim, J. H. and Kim, K. H. 2003. Effect of nanoparticles on critical heat flux of water in pool boiling heat transfer. *Applied Physics Letters*, Vol. 83, No. 16, 3374-3376.

You, S. M., Kim, J. H. and Kim, K. H. 2004. Pool Boiling Heat Transfer in Saturated Nanofluids. *Proceedings of IMECE 2004*, Anaheim, California, November 13-19.

Yu, W., and Choi, S. U. S. 2003. The Role of Interfacial Layers in the Enhanced Thermal Conductivity of Nanofluids: A Renovated Maxwell Model. *Journal of Nanoparticle Research,* vol. 5, pp. 167-171.

Yu, W., and Choi, S. U. S. 2004. The Role of Interfacial Layers in the Enhanced Thermal Conductivity of Nanofluids: A Renovated Hamilton-Crosser Model. *Journal of Nanoparticle Research,* vol. 6, pp. 355-361.

Yu, W., France, D. M., Routbort, J. L. and Choi, S. U. S. 2007. Review and Comparison of Nanofluid Thermal Conductivity and Heat Transfer Enhancements *Heat transfer Engineering* (submitted in July 2007)

Appendix A - Experimental procedure to run the nanofluid heat transfer test facility at ANL

The step by step experimental startup and shut-down procedures are described below.

Start-up and experimental testing procedures

1. Turn on computer data acquisition system.
   A. Click on the IBASIC icon. If the nanofluid data acquisition program starts, skip to step B to set the screen display. If the nucleate boiling data acquisition program starts, change to the nanofluid data acquisition program as follows. This procedure avoids an error condition and subsequent delay with the multiplexer.
      I. Enter a rotometer reading in the nucleate boiling data acquisition program when requested, e.g. 10.
      II. Let the program run, and listen to the clicks from the multiplexer. There will be two distinct clicks followed by a sequence of continuous clicks. While hearing the continuous clicks from the multiplexer, use the mouse to make the following choices: STOP, EDIT, FILE, OPEN, NANOSPHT.IBW, and RUN.
   B. Once the nanofluid data acquisition program starts, click on the ALPHA screen and then click on the GRAPH screen to set the display.

2. Turn on cooling water to the test facility by fully opening the SUPPLY and RETURN ball valves to the main manifold. Then partially open the two ball valves for supply and return from the main manifold to the test facility.
3. Turn on the preheater and the test section power supplies (the EMHP power supply for the preheater and the Sorensen 16-625T power supply for the test section).
    A. Set the voltage knobs to maximum (full clockwise rotation) on both power supplies.
    B. Set the current knobs to zero (maximum counter clockwise rotation) on both power supplies.
    C. Turn on the two power supply electrical disconnects (safety switches) on the wall to the left of the data-acquisition-system monitor.
    D. Turn on the main toggle switch on the Sorensen power supply.
    E. Push the white start button on the EMHP power supply.
4. Ready the pressure transducers.

The electronics for the test section absolute pressure and pressure drop are located above the data-acquisition-system monitor.

A. The two bridge units to the far left control absolute pressure. Zero the one on the left marked “Nanofluids” by pushing up on the AUTO toggle switch and holding it in that position for 5 seconds. The absolute pressure reading on the data-acquisition-system monitor should be close to 14.7 psia.
B. The Validyne unit on the far right (with the multimeter attached) controls the pressure drop transducer. With the span venire set to 1.84, zero the pressure drop using the multimeter as a guide and then the data-acquisition-system monitor for

the final reading. The pressure drop on the monitor should be within 0.02 psia of zero. Turn off the power to the multimeter.

5. Set the pump suction and discharge funnels, valves, and level conditions.
   A. The pump discharge funnel is located to the right of the pump. Set the liquid level to be within the pump output sight glass located below the funnel. Close the valve just below the funnel, and open the lower valve on the same vertical stainless steel tube. This setup provides flow pulse damping at the pump discharge.
   B. The pump suction funnel is located to the left of the pump. Valves on the vertical stainless steel tube below the funnel should be open with a liquid level in the funnel. This setup provides atmospheric pressure at the pump suction and an expansion reservoir for this system.
6. Start the test section flow with the pump controls.
   A. Turn on the pump power toggle switch.
   B. Set the flow direction. In the normal flow direction, the lower light is illuminated.
   C. Set the flow rate in ml/min with the up/down arrow controls. 500 ml/min is a good starting value for room temperature liquid.
   D. Press STOP/START.
7. Apply heat to the test section and the preheater.

In small increments, apply heat to the test section and preheater using the current knobs on the two power supplies.

To move to turbulent flow, slowly raise the current to 50 A at the test section and 30 A at the preheater over a period of 15 minutes. Then raise the flowrate to 880 ml/min and slowly raise the current to 110 A at the test section and 55 A at the preheater over a

period of 15 minutes. The approximate parameters at minimum turbulent flow are: mass flux = 3400 kg/m^{2}s, volumetric flowrate = 880 ml/min, test section inlet/outlet temperatures = 92˚C/100˚C, flowmeter temperature = 74˚C, test section current = 110 A, preheater current = 55 A, Reynolds number = 3200.

8. Set up the test.

Using the flow control on the pump, the test section and preheater power supplies, and the cooling water flow, set up the test.

9. Take data.

At steady state, as verified by the graphs on the data-acquisition-system monitor, press F8 on the data-acquisition-system computer. Follow the screen prompts to take data to the floppy disk. File names start with "N" followed by three numbers, e.g. N005.

10. After data is taken.

After data is taken by the data acquisition system, follow the screen prompt to TAKE MORE DATA even if you are about to shut down the system.

11. Set up for another test, or shut down the system.

Shut-down procedures

1. Reduce power.

Over a 15 minute period, slowly reduce to zero the power to the test section and the preheater by reducing the current to zero. During this process, slowly reduce pump flow to keep the test section pressure drop below 18 psia. It should not be necessary to go below 500 ml/min by this criterion.

2. After the test section and the preheater powers are at zero, turn off the electrical disconnects for the two power supplies. Keep the pump running at 500 ml/min until the maximum facility temperature (as shown on the data-acquisition-system monitor) is below 35 ˚C.
3. Turn off the pump power toggle switch.
4. Turn off cooling water valves SUPPLY and RETURN.
5. Turn off the data-acquisition-system computer controller.
   A. Click STOP, EDIT, CLOSE, and CLOSE WINDOWS.
   B. At the prompt C:\>, turn off the computer switch and the power strip switch.
   C. Remove the floppy disk with data.
6. Note that the power arrangement is such that the multiplexers always receive power. Be sure to maintain this condition.

Author's biography

Surya Kumar Saripella received his B.Tech. and M.Tech. in Mechanical Engineering from Indian Institute of Technology (IIT) Bombay, India in August 2006. Upon completion of his M.S. in Nuclear Engineering from University of Illinois at Urbana - Champaign, he is looking forward to pursuing a career in the financial industry with Quantum Phinance Consulting Pvt. Ltd., India.

Right from his childhood, Surya Kumar developed keen interest in sciences and excelled in every step of his education. Throughout his schooling, he consistently ranked among the top few of his class. He had been selected to appear for the Indian National Physics Olympiad (InPhO) and the Indian National Chemistry Olympiad (InChO).He was among the top 0.8 % of 125,000 students who took the Joint Entrance Examination (JEE) conducted for admission to the IITs (Indian Institute of Technology), the premier institutes of Engineering and Technology in India.

He was attracted towards Mechanical Engineering because of its fundamental nature and practical applicability in all spheres of life. His five years of undergraduate and graduate studies at IIT have exposed him to a wide gamut of subjects, including Solid Mechanics, Design, Controls, Dynamics, Thermal and Fluid Sciences, and other interdisciplinary programs, and this has created in him a fine overall blend of Engineering. He was specifically attracted towards the branch of numerical methods applied to solutions of engineering problems.

At the University of Illinois, along with excelling in the coursework as a graduate student, he also indulged himself in various projects related to flow visualization of two-phase flows through micro-channels with oil-holdup and has also been involved in developing semi-analytical models for two-phase flow through micro-channels. He also interned at the Argonne National Laboratory during summer 2007 along with the Energy Systems Division working on potential applications of nanofluids for “Class 8” Truck Diesel Engine cooling systems.